SEPTEMBER 2019 M.Sc. in Electrical and Electronics Engineering ABDURRAHİM MURATOĞLU


REPUBLIC OF TURKEY

GAZİANTEP UNIVERSITY

GRADUATE SCHOOL OF NATURAL & APPLIED SCIENCES


# RETRIEVAL OF EFFECTIVE CONSTITUTIVE PARAMETERS FOR BIAXIAL BIANISOTROPIC METAMATERIALS USING REFERENCE-PLANE-INVARIANT WAVEGUIDE METHOD

**M.Sc. THESIS**

**IN**

**ELECTRICAL AND ELECTRONICS ENGINEERING**

**BY**


**ABDURRAHİM MURATOĞLU**


**SEPTEMBER 2019**

# RETRIEVAL OF EFFECTIVE CONSTITUTIVE PARAMETERS FOR BIAXIAL BIANISOTROPIC METAMATERIALS USING REFERENCE-PLANE-INVARIANT WAVEGUIDE METHOD

**M.Sc. Thesis**

**in**

**Electrical and Electronics Engineering**

**Gaziantep University**

**Supervisor**

**Prof. Dr. Uğur Cem HASAR**

**by**

**Abdurrahim MURATOĞLU**

**September 2019**

REPUBLIC OF TURKEY
GAZİANTEP UNIVERSITY
GRADUATE SCHOOL OF NATURAL & APPLIED SCIENCES
ELECTRICAL AND ELECTRONICS ENGINEERING

Name of the Thesis : Retrieval of Effective Constitutive Parameters for Biaxial Bianisotropic Metamaterials Using Reference-Plane-Invariant Waveguide Method

Name of the Student : Abdurrahim MURATOĞLU

Exam Date : 04.09.2019

Approval of the Graduate School of Natural and Applied Sciences

Prof. Dr. A. Necmeddin YAZICI
Director

I certify that this thesis satisfies all the requirements as a thesis for the degree of Master of Science.

Prof. Dr. Ergun ERÇELEBİ
Head of Department

This is to certify that we have read this thesis and that in our consensus opinion it is fully adequate, in scope and quality, as a thesis for the degree of Master of Science.

Prof. Dr. Uğur Cem HASAR
Supervisor

| Examining Committee Members: | Signature |
|---|---|
| Prof. Dr. Uğur Cem HASAR | ………………….. |
| Prof. Dr. Kemal DELİHACIOĞLU | ………………….. |
| Asst. Prof. Dr. Musa BUTE | ………………….. |

**I hereby declare that all information in this document has been obtained and presented in accordance with academic rules and ethical conduct. I also declare that, as required by these rules and conduct, I have fully cited and referenced all material and results that are not original to this work.**

**Abdurrahim MURATOĞLU**

# ABSTRACT

**RETRIEVAL OF EFFECTIVE CONSTITUTIVE PARAMETERS FOR BIAXIAL BIANISOTROPIC METAMATERIALS USING REFERENCE-PLANE-INVARIANT WAVEGUIDE METHOD**

**MURATOĞLU, Abdurrahim**
**M.Sc. in Electrical and Electronics Engineering**
**Supervisor: Prof. Dr. Uğur Cem HASAR**
**September 2019**
**65 pages**

This study is about electromagnetic characterization of bi-axial bianisotrpic metamaterials. Rectangular waveguide method is used to extract scattering parameters in microwave X-band frequency region. In general, by these techniques it is presumed that the measurement and reference planes of specimen are overlapped which can cause errors otherwise. Reference-plane-invariant technique is investigated for the extraction of the effective constitutive parameters. By this technique, the measurements, can be performed without precise knowledge of the positions of the measured specimen reference planes. The study is validated by comparing extracted constitutive parameters with a method requiring reference plane position of the measured slab. As a preliminary, the concept is simulated by a commercial electromagnetic field simulation software. The results obtained by simulations are reinforced with physical waveguide experiments by using a vector network analyzer. For the measurement experiments, split-ring-resonator type metamaterials are designed, fabricated and used.



**Key Words:** Electromagnetic Characterization, Reference-Plane-Invariant (RPI), Scattering (S-) Parameters, Rectangular Waveguide Method, Metamaterial

# ÖZET

## RETRIEVAL OF EFFECTIVE CONSTITUTIVE PARAMETERS FOR BIAXIAL BIANISOTROPIC METAMATERIALS USING REFERENCE-PLANE-INVARIANT WAVEGUIDE METHOD

**MURATOĞLU, Abdurrahim**
**Yüksek Lisans Tezi, Elektrik – Elektronik Mühendisliği**
**Danışman: Prof. Dr. Uğur Cem HASAR**
**Eylül 2019**
**65 sayfa**

Bu çalışma, biaksiyal bianizotropik metamalzemelerin elektromanyetik karakterizasyonu üzerinedir. Mikrodalga X-bandı frekansında, saçılma parametrelerini elde etmek için dikdörtgen dalga kılavuzu metodu kullanılmıştır. Genellikle bu teknikler, ölçüm düzlemlerinin ve ölçülen örneğin dayanak düzlemlerinin üst üste gelmesi şeklinde çalışır. Aksi takdirde ölçüm hataları ortaya çıkabilir. Yapısal parametreleri elde etmek için dayanak-düzlem-değişimsiz yöntemi araştırılmıştır. Bu yöntemle, ölçümler numunenin dayanak düzlem bilgileri olmadan gerçekleştirilebilir. Bu çalışma, ölçülen örneğin dayanak-düzlem bilgisini gerektiren başka bir yöntemle elde edilen yapısal parametrelerin karşılaştırılması ile doğrulanmıştır. İlk olarak, ticari bir elektromanyetik alan benzetim programı kullanılarak benzetimler gerçekleştirilmiştir. Benzetimlerden elde edilen sonuçlar, bir vektör – ağ çözümleyici cihazı kullanılarak yapılan fiziksel dikdörtgen dalga kılavuzu deneyleri ile pekiştirilmiştir. Deneylerde kullanılmak üzere, yarık-halka-kovuğu şeklindeki metamalzemeler tasarlanıp üretilmiştir.

**Anahtar Kelimeler:** Elektromanyetik Karakterizasyon, Dayanak-Düzlem-Değişimsiz, Saçılma Parametreleri, Dikdörtgen Dalga Kılavuzu, Metamalzeme

*"Dedicated to my family"*

## ACKNOWLEDGEMENTS

I would like to express my deepest gratitude to my supervisor Prof. Dr. Uğur Cem Hasar for his support, guidance, advice, criticism, encouragements and insights throughout the study. Similarly, I would like to thank to Asst. Prof. Dr. Musa Bute for his support and guidance.

I would like to thank to the Scientific and Technological Research Council of Turkey (TUBITAK) for the support provided under the project 112R032.

Last and most, I would like to thank my beloved mother, father and siblings for everything they have done in my whole life. Especially, I would like to thank my dear wife Elif who supported, motivated me all the time and put up with me throughout the study.

# TABLE OF CONTENTS

# LIST OF TABLES

**Page**

## LIST OF FIGURES

**Page**

## LIST OF SYMBOLS

| | |
|---|---|
| $\varepsilon$ , $\mu$ | Electric Permittivity and Magnetic Permeability |
| $\bar{\boldsymbol{\varepsilon}}$ , $\bar{\boldsymbol{\mu}}$ | Elec. Permittivity and Mag. Permeability Tensors |
| **E** | Electric Field Intensity |
| **H** | Magnetic Field Intensity |
| **D** | Electric Flux Density |
| **B** | Magnetic Flux Density |
| **J** | Current Density |
| $\rho$ | Charge Density |
| $k$ | Wavenumber |
| **k** | Wave Propagation Vector |
| **P** | Poynting Vector |
| $c$ | Speed of Light in Vacuum |
| $n$ | Refractive Index |
| $k$ | Wavenumber |
| $\omega$ | Angular Frequency |
| $S_{11}$ | Forward Reflection Coefficient |
| $S_{21}$ | Forward Transmission Coefficient |
| $S_{22}$ | Backward Reflection Coefficient |
| $S_{12}$ | Backward Transmission Coefficient |
| $\varsigma$, $\zeta$ | Cross Coupling Terms |
| $\Gamma_1, \Gamma_1$ | Semi-infinite Reflection Coefficients |
| T | Propagation Factor |
| $z_{ws}^{+}$ , $z_{ws}^{-}$ | Normalized Forward and Backward Wave Impedances |
| $\beta_{sz}$ | Phase Constant in $z$-direction Through a Sample |
| $\beta_{0x}$, $\beta_{0z}$ | Phase Constant in $x$ and $z$ Directions Through Air |
| $f$ | Frequency |

# LIST OF ABBREVIATIONS

| | |
|---|---|
| **MM** | Metamaterial |
| **RPI** | Reference-Plane Independent |
| **RPD** | Reference-Plane Dependent |
| **LHM** | Left-Handed Media/Material |
| **SRR** | Split-Ring Resonator |
| **ELC** | Electric Inductive-Capacitive |
| **VNA** | Vector Network Analyzer |
| **DPS** | Double Positive |
| **SNG** | Single Negative |
| **ENG** | Epsilon Negative |
| **MNG** | Mu Negative |
| **DNG** | Double Negative |
| **S-** | Scattering |
| **CST** | Computer Simulation Technology |
| **ABCD** | Transmission Matrix |
| **PCB** | Printed Circuit Board |
| **TRL** | Through-Reflect-Line |

# CHAPTER 1

# INTRODUCTION

## 1.1 Introduction to Metamaterials

In 1967, V.G. Veselago [1] pave the way for starting the age of new artificial materials by studying substances simultaneously having negative valued electric permittivity $(\varepsilon)$ and magnetic permeability $(\mu)$ which do not exist in the nature. These artificial materials which is also called engineered materials, commonly entitled as Meta-materials. The word "meta" of Greek origin gives meaning the beyond. In fact, the metamaterials (MM) have exotic and interesting electromagnetic features that the conventional materials existing in the nature do not have. Negative group velocity, negative refractive index and reverse Doppler effect phenomena are among them. MMs are also important to be appeared in applications in electromagnetics such as sensors [2], absorbers [3], electromagnetic cloaking [4] and antenna directivity manipulations [5].

Almost 30 years later the theoretical demonstration of MMs by Veselago, in 1996 J. B. Pendry and his colleagues [6] experimentally demonstrated a medium having negative $\varepsilon$ utilizing periodic structures built of very thin wires. Similarly, in 1999 Pendry et al. [7] showed negative $\mu$ by producing and utilizing structures composed of conducting nonmagnetic micro split-ring resonators. Eventually, in 2000 Smith et al. [8] manifested a composite medium with simultaneously negative $\varepsilon$ and $\mu$ that consists of periodically interspaced conducting nonmagnetic split-ring resonators and continuous wires. The dimensions of micro cells that form the metamaterial structure is much less than the wavelength of the propagating electromagnetic field through the media.

## 1.2 Motivation

We live in such a world that is fully combined of different types of materials that each have different physical, chemical, electrical, electromagnetic, etc. properties, characteristics and structures. Materials exist in the nature as pure elements, compounds or as mixture forms. They have different states (solid, liquid, gas and plasma) in different environmental conditions. Materials are used for many different purposes at many different application areas such as engineering, technical, medical, optical, economical fields and etc., depending on their nature and characteristic properties. It is possible to tell that the nature of materials is determined by their constitutive parameters or vice versa. For this reason, specific constitutive parameters of materials should be well measured, disclosed and compared. Thus, measurement methodologies and techniques, have a great importance in science and technology.

Although measurement related concepts date back to ancient times, after the second half of nineteenth century, the measurement studies became a separate field of science [9]. Together with the scientific and technological advances, the measurement sciences have evolved and throve. Many measurement methodologies, techniques and instruments have been invented and improved in many different fields. As a field, Electromagnetics is one of the most important part of the measurement science. In today's digitalized world, technology and accordingly daily life is mostly dependent on the electronics based systems and thus, this situation necessitates electromagnetic characterization of materials. The electromagnetic characterization of materials is needed to be performed prior their use in microwave and in many other applications such as wireless communication, radar, navigation, electronic circuits, power systems, transmission lines, medical equipment, pharmaceutical and etc. [10].

In addition to the investigation and characterization of conventional materials, after the emergence of MMs into the real world, they drew the attentions for electromagnetic measurements and characterization. The measurement science played a key role in the improvement of MMs. Because, the applications of MMs such as, sensors, absorbers, antennas, perfect lens and electromagnetic cloak directly depends on electromagnetic constitutive parameters of MMs which should be revealed. Although, the history of MMs dates back to 1967, the field may be counted young, and still hot since the fabrication of first MMs about the year 2000.

## 1.3 Literature Review

Various measurement methods are proposed to characterize electromagnetic parameters of MMs. The studies on MM measurement techniques can be enumerated as; field averaging, qualitative effective medium theory, homogenization and scattering (S-) parameter extraction. In the first method [11], the ratio of electric and magnetic fields is calculated numerically at the surfaces and edges of MM structures. Although, it is favorable for numerical simulations, it is not applicable for experimental measurements. In the qualitative effective medium theory [12,13], approximate analytical and dispersive models are obtained by optimization and used. The method provides pretty accurate results for simple structured MMs, but for complex structures the method may lose precision. As a third, various homogenization methods are proposed including curve fitting, field averaging, dispersion equation techniques [14,15]. Finally, S-parameters method is the mostly and widely employed technique. The technique is applicable for both electromagnetic simulations and experimental measurements.

There exist numerous methodologies for extraction of S-parameters in the literature. The methods to be applied may vary by the properties of sample structure, size, type, frequency range, measurement expectations and etc. Each has its own advantages-disadvantages, conveniences-limitations and etc. The resonator method, the coaxial probe method, the free-space method and the rectangular waveguide method are commonly used techniques that utilizes S-parameters extraction to characterize electromagnetic properties of measured materials.

In resonator techniques, resonant frequency and quality factor of resonating modes alterations are measured before and after the insertion of samples. It gives very precise and accurate results but generally it is not used by itself only. Rather, the technique is used together with other non-resonant measurement techniques. In other words, the constitutive parameters of samples are measured with non-resonant methods for a wide frequency range and then, utilizing the resonator method, the constitutive parameters are obtained for very narrow frequency ranges. In brief, it is constrained to single or several frequencies which makes the method inconvenient for MM characterization. Also, since the method necessitates intricate and elaborative preparation of samples, the process gets harder and more expensive [16].

The coaxial probe method allows wide frequency band measurements which is very advantageous. The uncertainties due to errors in the structure of measured samples are not determinant. Any size of samples can be used, providing that, they are produced in cylindrical or toroidal shape [17,18]. Unfortunately, the geometry requisite is very constraining for measurements of MMs.

The free-space measurement method can be performed in a wider frequency range which is advantageous over the other methods. For the measurement, different kinds of samples and antennas can be used. But the best results are obtained when normally incident plane waves are directed onto the planar samples. Unfortunately, the method is receptive to errors and measurements may be exposed to environmental influences such as electromagnetic disturbances. In addition, for the application of the method, the measurements must be taken very sensitively and precisely. Moreover, greater sample preparation is needed especially for periodic structures or MMs which causes increased fabrication costs. Shi et al. [19] and Smith et al. [20] performed electromagnetic parameter retrieval for inhomogeneous MMs. Hasar et al. [21] submitted a paper analyzing isotropic MMs involving boundary effects. Jiang et al. [22], Discroll et al. [23] and Menzel et al. [24] analyzed extraction of constitutive parameters for anisotropic MMs. In addition, these methods are studied in [25-29] for the analysis of bianisotropic MMs.

The rectangular waveguide method is a commonly and widespread technique used in microwave measurements. It is relatively easier and simpler to perform the measurements. It is not sensitive to external disturbances due to inserting samples into waveguides. Each waveguide has a range of working frequencies. Some of them are wide or narrow which is dependent on waveguide dimensions. Thus, suitable waveguides must be chosen for the desired frequency range. Moreover, usually the sample production is quite easier. Because the measurements are performed using samples with small cross section areas to fit inside waveguides. Especially, the technique is very useful and facilitative for metamaterial measurements due to imaging effect of the conducting waveguide walls. The electromagnetic properties of a large-scale structure can be obtained by measuring just a small slab of sample using waveguide method. Hasar et al. [30,31] researched low-loss isotropic MMs for constitutive parameters retrieval by using rectangular waveguide method. Trang et al.

[32] extracted constitutive parameters of high temperature superconducting, anisotropic MM and Chen et al. [33] presented a study on measurement of complex permittivity and permeability tensors of anisotropic MMs. Also, Hasar et al. proposed waveguide methods for strongly and weakly coupled bianisotropic MMs [34,35].

In general, it is assumed that the reference plane i.e. calibration plane is overlapped with the measurement plane (the physical surface of measured slab) [19,20,25,26,28,29,34-35]. Unfortunately, this circumstance may cause some measurement faults in the calculated constitutive parameters of measured sample in the case of misplacement of the planes especially in at higher frequency regimes [37]. Also, it may be troublesome to critically adjust the position of the sample. In order to avoid this situation, some methods called reference plane invariant (RPI) are proposed for conventional isotropic materials [38-42], for isotropic MMs [21,43]. In addition, an RPI method is proposed for uniaxial bianisotropic MMs [37]. Nevertheless, this method is not suitable for electromagnetic characterization of biaxial bianisotropic MMs. To the best of our knowledge, no method is proposed for the extraction of effective constitutive parameters of biaxial bianisotropic MMs.

## 1.4 Outline of the Thesis

In Chapter 1, the introductory information about the metamaterials and the motivation for the thesis are presented. A literature survey on the measurement methodologies for electromagnetic characterization of MMs is reported.

In Chapter 2, a brief theory of MMs is introduced. The materials are classified with respect to electric permittivity and magnetic permeability and properties of different electromagnetic materials are discussed with the interaction of electromagnetic waves in these media. After, the homogeneity and isotropy of the materials are referred. Also, the excitation techniques of MM structures are discussed. Towards the end of the chapter, the description of the problem is presented. Finally, the method to obtain effective constitutive parameters of biaxial bianisotropic MMs via RPI method through waveguide measurements is proposed and the retrieval process is given in detail.

In Chapter 3, a bianisotropic MM unit cell and MM structure consisting of dielectric substance and split-ring resonators (SRR) is designed to be analyzed in this study and the geometrical and constructional properties are reported. After, a 3D electromagnetic simulation environment is introduced with the prepared MM slab and assigned simulation setup. Next, the proposed method is validated using the S-parameters obtained by the performed numerical simulations and compared with a method requiring reference-plane information. Finally, validation of the method is also performed by the data obtained from experimental measurements of fabricated MM sample. Results from simulations and measurements are compared and reported.

In Chapter 4, general conclusion remarks about the study and proposed method are presented.

## 1.5 Contributions

The main contribution of this thesis is a proposed method of a reference-plane-invariant for waveguide measurements of biaxial bianisotropic MMs. By this method, the electromagnetic properties of such kind MMs could be retrieved without requiring position location of measurement planes. The outcomes of the thesis research are published as an international journal paper [60].

Throughout my thesis studies, I had opportunities to join and contribute in various research works under the supports of the Scientific and Technological Research Council of Turkey (TUBITAK) under projects 112R032 and 114E495 and these studies are published in several international journal papers [26,34,72].

# CHAPTER 2

# THEORY AND METHODOLOGY

In this chapter, a general theory of MMs is given. Classification of materials with respect to electric permittivity and magnetic permeability is provided. Some properties of MMs are mentioned. Description of the problem is submitted and reference-plane-invariant waveguide characterization technique for biaxial bianisotropic MMs is proposed. Finally, de-embedding technique is briefly mentioned which is used for the analyzes.

## 2.1 Theory of Metamaterials

Electric permittivity ($\varepsilon = \varepsilon_0 \varepsilon_r$) and magnetic permeability ($\mu = \mu_0 \mu_r$) are two basic constitutive parameters that specify the propagation of electromagnetic waves in a medium, since they identify the refractive index of a material and the dispersion equation, accordingly. The refractive index ($n$) of a material may be written as:

$$n = \sqrt{\varepsilon_r \mu_r} \tag{2.1}$$

Accordingly, the refractive index for an isotropic medium can be expressed as:

$$n^2 = k^2 \frac{c^2}{\omega^2} \tag{2.2}$$

where $k$ is the wavenumber and $\omega$ is the angular frequency of the propagating electromagnetic wave. Also, the speed of light in vacuum is symbolized with $c$.

If the medium is assumed to be simple (linear, homogenous, isotropic) and lossless, accordingly, $n$, $\varepsilon$, $\mu$ parameters become real. As it can be seen, in the case of simultaneously negative $\varepsilon$ and $\mu$, this negativity has no effect on dispersion relation [1]. However, the case has some effects on Maxwell's equations and it should further be analyzed.

To understand electromagnetic wave and medium interaction, the Maxwell's equations should be investigated correctly. Since, electromagnetic waves satisfy the Maxwell's equations in terms of space and time variables may be written as:

$$\vec{\nabla} \times \mathbf{E} = -\frac{\partial \mathbf{B}}{\partial t} \tag{2.3}$$

$$\vec{\nabla} \times \mathbf{H} = \frac{\partial \mathbf{D}}{\partial t} + \mathbf{J} \tag{2.4}$$

$$\vec{\nabla} \bullet \mathbf{D} = \rho \tag{2.5}$$

$$\vec{\nabla} \bullet \mathbf{B} = 0 \tag{2.6}$$

where **E** and **B** are electric and magnetic field intensities. Assuming the medium is simple i.e. linear, homogenous and isotropic then $\varepsilon_r$ and $\mu_r$ possess real values. Thus, the electric and magnetic flux densities given in Equations (2.3 – 2.6) may be written in terms of **E** and **H** for a simple medium as:

$$\mathbf{D} = \varepsilon \mathbf{E} \qquad \left(\mathrm{C/m^2}\right) \tag{2.7}$$

$$\mathbf{B} = \mu \mathbf{H} \qquad (\mathrm{T}) \tag{2.8}$$

Also, the relation between current density (**J**) and volume charge density ( $\rho$ ) may be written as:

$$\vec{\nabla} \bullet \mathbf{J} = -\frac{\partial \rho}{\partial t} \tag{2.9}$$

To simplify the investigation, uniform plane wave propagation is assumed and the field intensities are expressed in phasor domain by using $e^{i\omega t}$ convention, as:

$$\mathbf{E}(R) = \mathbf{E}_0 e^{-j\mathbf{k}\cdot\mathbf{R}} \qquad (\text{V/m}) \tag{2.10}$$

$$\mathbf{H}(R) = \mathbf{H}_0 e^{-j\mathbf{k}\cdot\mathbf{R}} \qquad (\text{A/m}) \tag{2.11}$$

where $\mathbf{k}$ is the wavenumber vector and $\mathbf{R}$ is the radius vector. Inserting the Equations (2.10) and (2.11) into Equations (2.3) and (2.4), for the plane and monochromatic wave, the Maxwell's equations are reduced to:

$$\mathbf{k} \times \mathbf{E} = -\omega\mu\mathbf{H} \tag{2.12}$$

$$\mathbf{k} \times \mathbf{H} = \omega\varepsilon\mathbf{E} \tag{2.13}$$

It can be realized that, if $\varepsilon$, $\mu$ are positive at the same time, then **k**, **E** and **H** constitutes a right-handed set of vectors. Conversely, in the case of simultaneous negative $\varepsilon$, $\mu$ they constitute a left-handed set of vectors [1]. That means a backward propagating of electromagnetic wave which sounds interesting. In addition, a media that has positive $\varepsilon$ and $\mu$ together is called double-positive (DPS) and contrarily a media of simultaneous negative $\varepsilon$ and $\mu$ is called double-negative (DNG) media.

Moreover, investigating the Poynting vector (**P**) which refers to energy flow density and direction, may be expressed as follows:

$$\mathbf{P} = \mathbf{E} \times \mathbf{H} \qquad (\text{W/m}^2) \tag{2.14}$$

The Poynting vector **P** is not dependent on the signs of the constitutive parameters. Therefore, **P** forms a right-handed set together with **E** and **H**. Thus, the direction of energy flow density is not reversed even with a backward propagating electromagnetic wave in a DNG media. Briefly, **k** and **P** vectors show the same direction in DPS media and the opposite directions in DNG media. This phenomenon is illustrated in Figure 2.1.

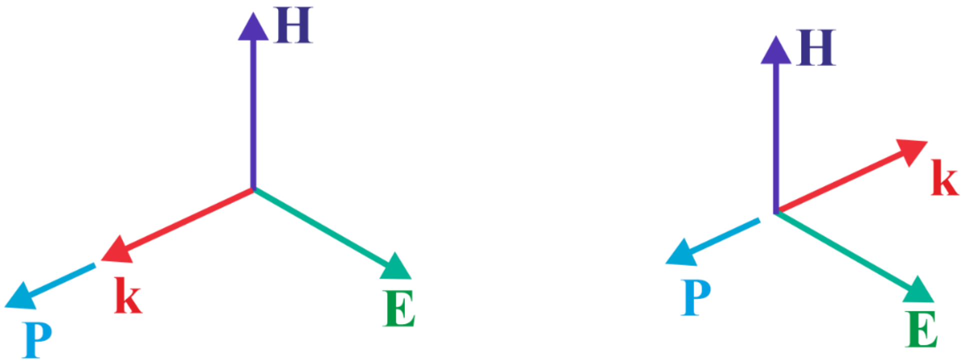


**a)** Right-handed medium $\varepsilon > 0$, $\mu > 0$ **b)** Left-handed medium $\varepsilon < 0$, $\mu < 0$

**Figure 2.1** Illustration of k, E, H and P vectors for RHM and LHM

Since the direction of **k** is same with the direction of group velocity, Veselago remarked that, left-handed material term is equivalent to material with negative group velocity [1].

## 2.2 Classification of Metamaterials

It is sensible to classify the MMs with respect to signs (positive and negative) of constitutive parameters, $\varepsilon$ and $\mu$. Since the $\varepsilon$ and $\mu$ each may possess two signs and four different combinations in total. Therefore, for each case materials will have different electromagnetic characteristics.

Nearly all isotropic materials having simultaneously positive values of $\varepsilon$ and $\mu$ ($\varepsilon > 0$, $\mu > 0$) such as conventional materials and artificial dielectrics [44,45]. Therefore, this kind of materials are named as double positive (DPS) materials. Also, materials having either negative $\varepsilon$ or $\mu$ are entitled as single negative (SNG) medium and they can be further categorized according to the negativeness of the parameters as epsilon-negative (ENG) and mu-negative (MNG). An illustration of classification of MMs is given in Figure 2.2.

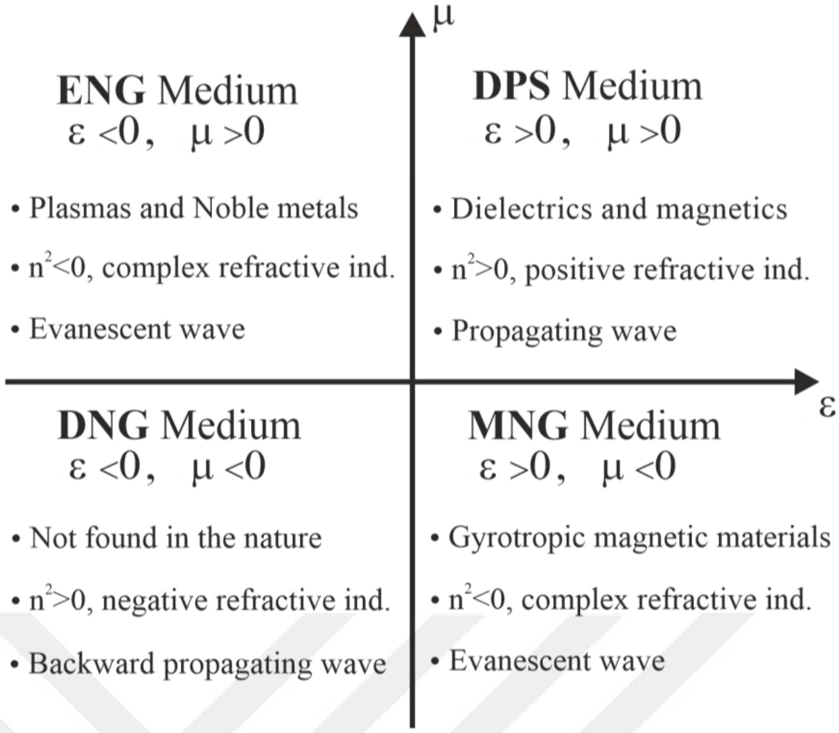


**Figure 2.2** Classification of MMs by the sign of $\varepsilon$ and $\mu$ [44,46]

### 2.2.1 Single-Negative Medium (SNG)

There are two kinds of SNG medium; either having negative permittivity or negative permeability. Due to this reason the square of refractive index will be multiplication of effective permittivity and permeability of the medium:

$$n = \sqrt{\varepsilon_{eff}\mu_{eff}} \tag{2.15}$$

Thus, the refractive index will be pure imaginary. Also, rearranging the Equation (2.2):

$$k = n\frac{\omega}{c} \tag{2.16}$$

In SNG media, the propagation constant will be imaginary. Thus, the electromagnetic waves in SNG medium will be evanescent.

#### 2.2.1.1 Epsilon-Negative Medium (ENG)

ENG materials having negative permittivity and positive permeability values ($\varepsilon < 0$, $\mu > 0$). ENG materials involve plasma and plasmonic materials such as noble metals and some polar dielectrics [44,71]. The ENG materials also include MMs. Pendry et al. [6,47] demonstrated negative permittivity but positive permeability MMs composed of thin metal wires below the plasma frequency. The wires of the structure are aligned parallel to the electric field component of electromagnetic wave and it is illustrated in Figure 2.3. An ENG material can also be realized by split ring resonator (SRR) and electric LC resonators (ELC) beside the thin wire structures [55]. The SRRs are circular or rectangular shaped single or coaxial rings that have small splits. The structures are stimulated by electric excitation and there exist numerous resonator geometries that is used in the literature [48-51]. The geometries, dimensions of resonators and distances between resonators and thin wires are important parameters determining the value of electric permittivity. There is also another structure (isotropic) of triple-wire constituting negative permittivity medium [52].

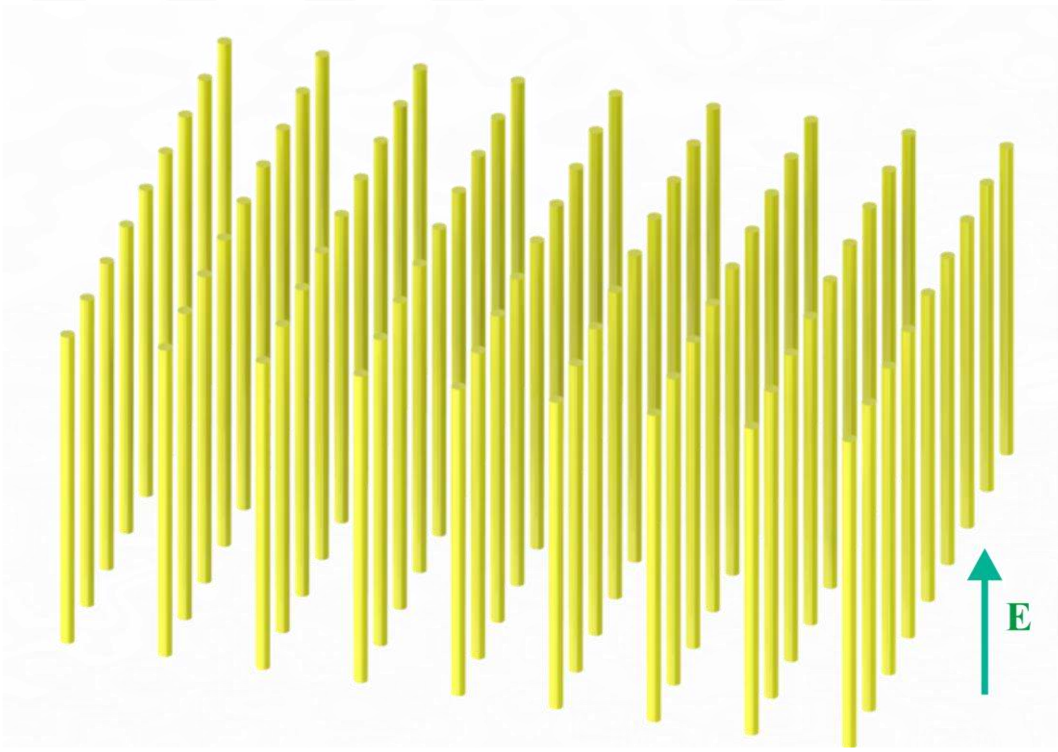


**Figure 2.3** A Structure of periodic thin wires having negative permittivity value

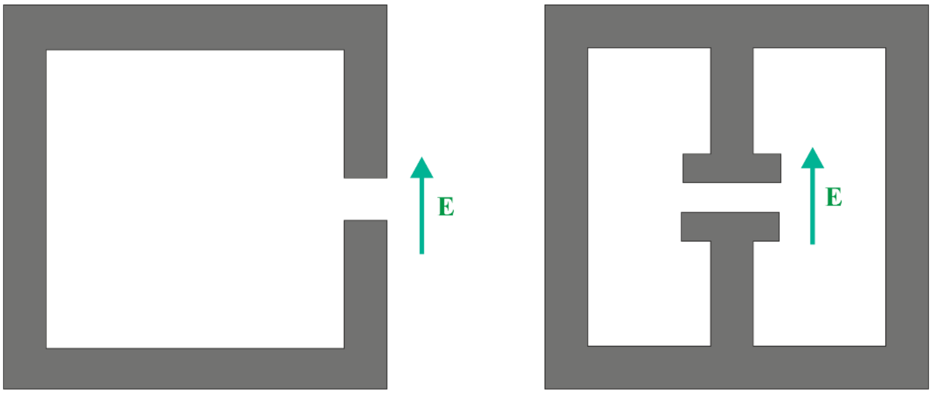


(a) (b)

**Figure 2.4** Frontal view of MM resonators having negative permittivity values. ***a)*** *Single SRR structure* ***b)*** *ELC structure*

#### 2.2.1.2 Mu-Negative Medium (MNG)

Above, negative permittivity possessing structures made out of metallic thin wires and SRRs are reported. Here, materials having negative mu but positive epsilon are discussed ($\varepsilon > 0$, $\mu < 0$). Due to the absence of magnetic charges it is comparatively harder to obtain negative permittivity materials [53]. Pendry et al. introduced nonmagnetic conducting SRR structures having negative permeability near resonance frequency [7]. Negative permeability is achieved by the excitation of magnetic field that directed perpendicularly to the plane of SRRs. Capacitive elements of the microstructures such as splits and gaps causes resonances and accordingly positive and negative permeability values about the resonance frequency [53]. SRR structures, spiral, S and Ω shaped resonators and Swiss roll capacitor are among different types of MM structures that form a MNG media [44]. Some forms of MNG MM structures are depicted in Figure 2.5.

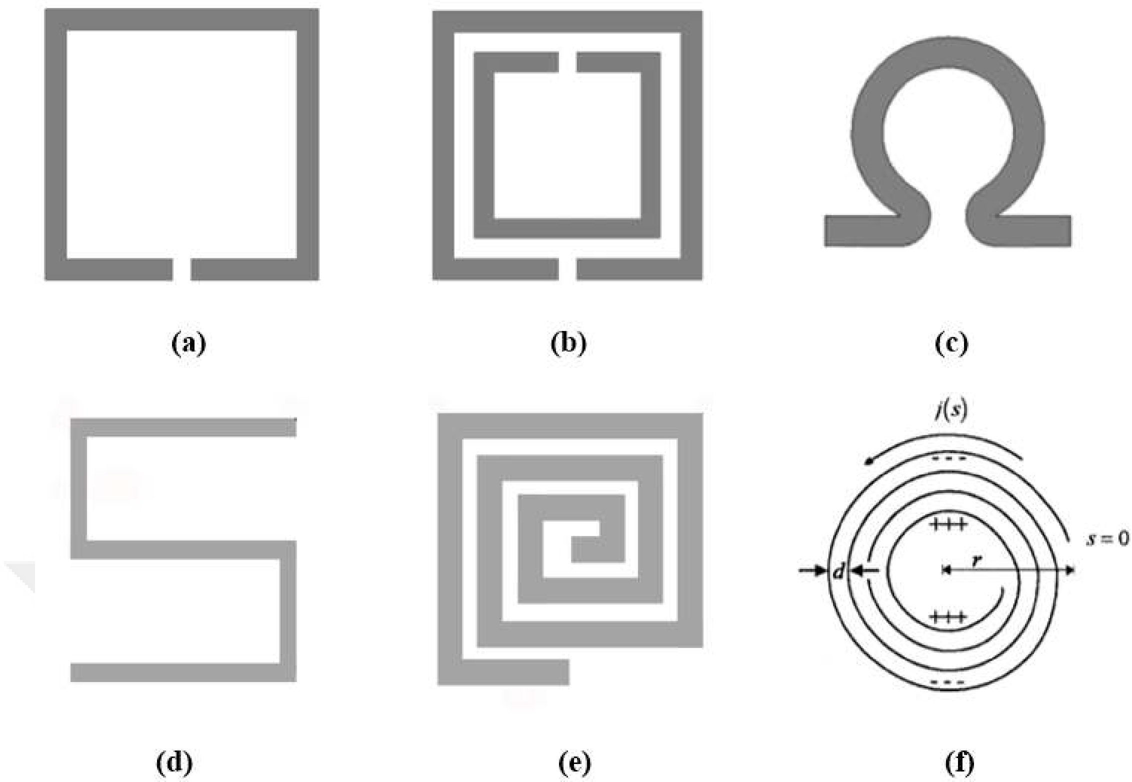


**Figure 2.5** MM structures forming MNG media. ***a)*** *Single rectangular SRR* [44] ***b)*** *Coaxial rectangular SRR* [44] ***c)*** *Omega-shaped resonator* [37] ***d)*** *S-shaped resonator* [44] ***e)*** *Spiral–shaped resonator* [44] ***f)*** *Swiss-roll capacitor* [7]

### 2.2.2 Double Negative Medium (DNG)

DNG materials do not exist in the nature and they simultaneously have negative permittivity and permeability ($\varepsilon < 0$, $\mu < 0$). The SNG and DNG materials have been realized thanks to the advancement in materials science. DNG materials are also called left-handed media or negative-index materials. Due to negative refractive index, these materials have exotic electromagnetic characteristics. A DNG material may be formed simply by combining structures of ENG and MNG materials. To the best of our knowledge, the first experimental research [8] on DNG materials has been announced by Smith et al. They produced this composite MM structure by combining SRRs and continuous wires. A MM structure composed of SRRs and thin wires is shown in Figure 2.6.

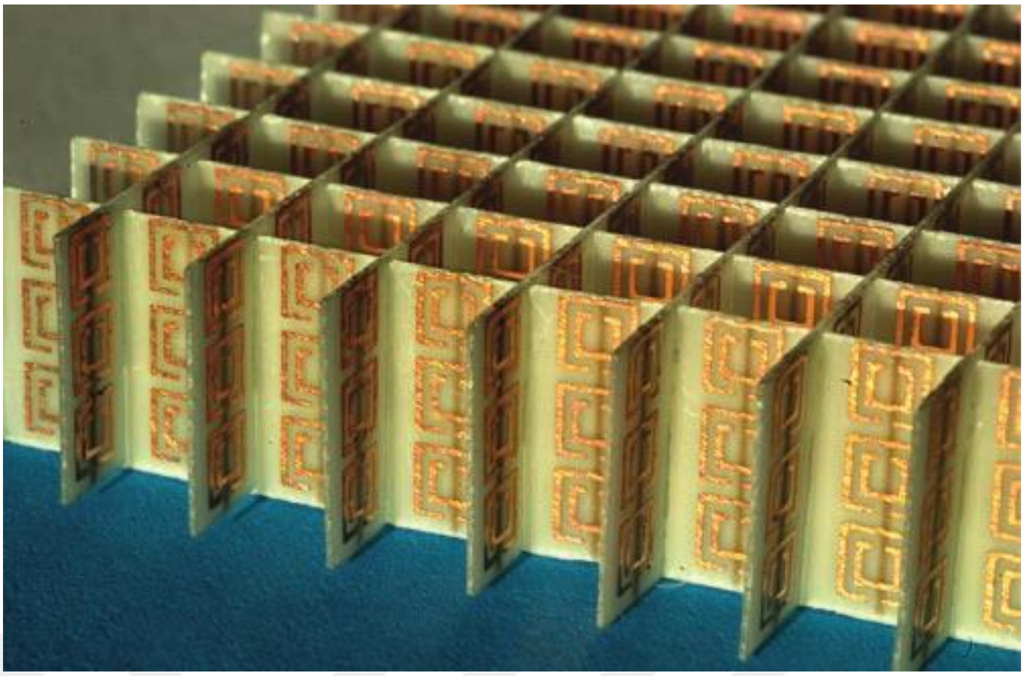

**Figure 2.6** A MM structure having simultaneously negative $\varepsilon$ and $\mu$ [54]

Thin wire structure is used to form ENG and DNG media even for a wider range, however, it is not the only way to constitute DNG material. A composite medium composed of SRRs that have electrical and magnetic excitation may also have left-handed property [50]. After the emergence of the DNG MMs many numerical and experimental studies have been conducted and numerous types of DNG MM structures are proposed.

## 2.3 Negative Refractive Index

Travelling electromagnetic or optical waves expose to refraction while passing through different media. The refraction relation between incidence angle of propagating wave and refractive index of medium is explained by well-known Snell's Law. It may be shown as:

$$\frac{n_1}{n_2} = \sqrt{\frac{\varepsilon_1\mu_1}{\varepsilon_2\mu_2}} = \frac{\sin\phi}{\sin\theta} \tag{2.17}$$

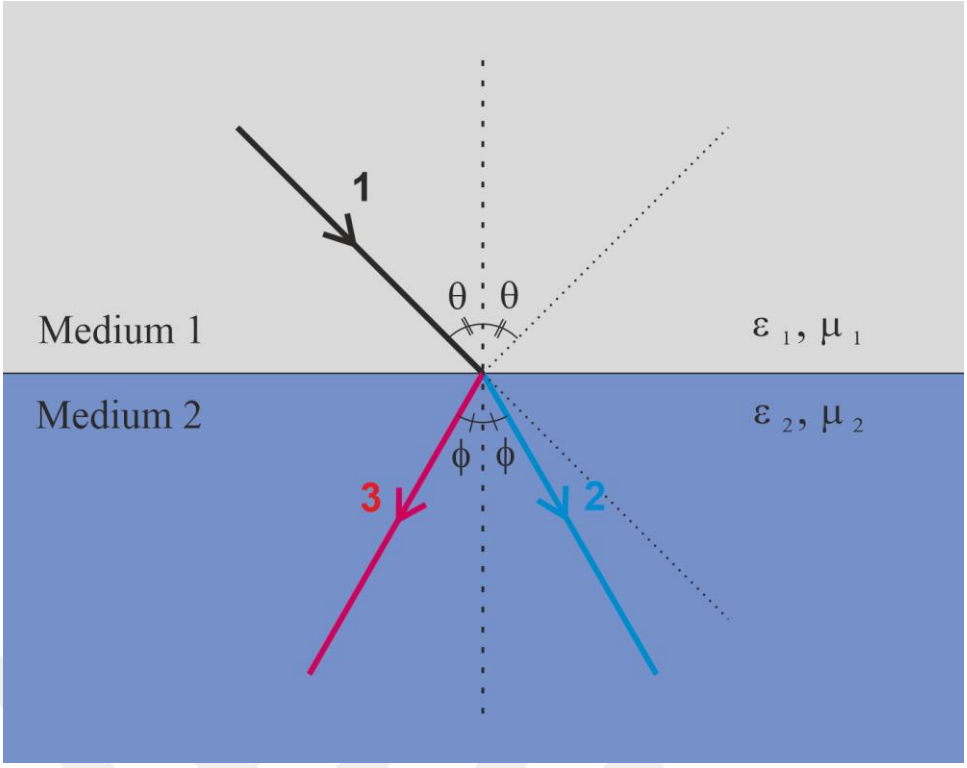


**Figure 2.7** Wave refraction between two different media

If both media are composed of DPS substances, the refractive indexes will be positive and the incident wave coming through $1^{st}$ path will be refracted and will follow the $2^{nd}$ path. However, if the wave is transmitted from a DPS medium to a DNG medium, the refraction happens in an extraordinary way and the wave follows the $3^{rd}$ path. The phenomenon is illustrated in Figure 2.7. Additionally, if either $\varepsilon$ or $\mu$ is negative, then the refractive index will be pure complex and the wave will not propagate.

## 2.4 Excitation of Split-Ring-Resonator (SRR) MMs

The SRR type MMs are very commonly used in MM applications since they could be designed to obtain ENG, MNG and DNG type structures. For example, negative permittivity could be obtained without using thin wire arrays which makes SRRs practical. In order to comprehend the electromagnetic medium characteristics of SRR MM structures, the excitation techniques of SRR must be apprehended. SRR structures can be excited in three ways; electric, magnetic and both electric-magnetic excitations. The way of excitations is subject to the application requirements of SRR structures.

To obtain ENG type media, the SRR structures should be electrically excited only. By electrical excitation, electric charges are deposited or accumulated at the edges of SRR structures. Thus, charge densities with opposite polarities are induced which causes electric dipole. Similarly, to obtain MNG type media, the SRR structures should be excited magnetically only. Magnetic field of propagating wave through the media, generates a magnetic dipole by inducing circulating currents in the surface of metallic parts of SRR structures. Finally, to obtain DNG type media, the SRR is stimulated by the combination of two ways. These conditions are illustrated in Figure 2.8 [55].

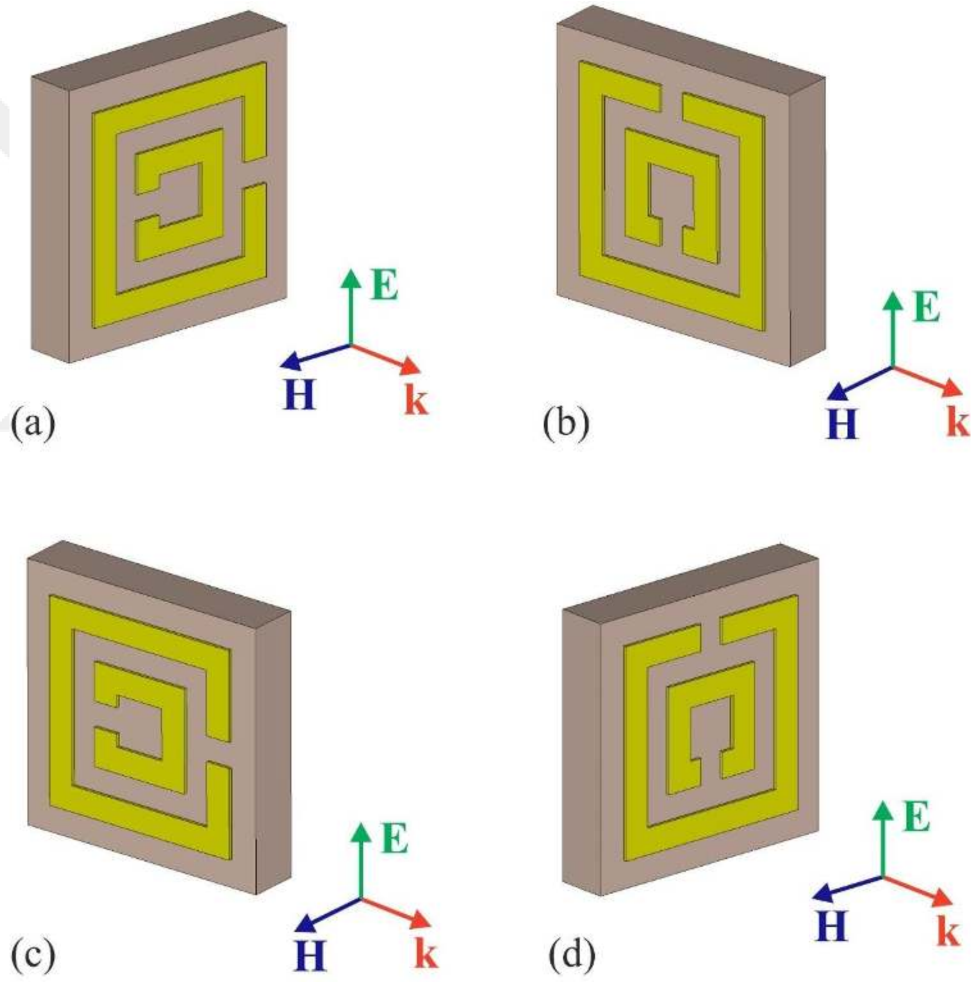


**Figure 2.8** SRR structures and exposed electromagnetic fields

In Figure 2.8 (a), the electric excitation occurs since the electric field component of propagating wave is perpendicular to splits of the resonator. The magnetic field is ineffective since it is not perpendicular to the SRR plane, i.e. it is not passing through the resonator ring structure to induce circulation currents as explained in Faraday's law of induction. In Figure 2.8 (b) magnetic excitation takes place since, only magnetic field is directed in an effective way. In Figure 2.8 (c), both electric and magnetic excitation occurs and in Figure 2.8 (d) there is neither electric nor magnetic excitation, because the fields are directed in ineffective manners.

## 2.5 Medium Homogeneity and Isotropy

**Homogeneity** of a medium describes uniformity and regularity of a medium at every point implied. MMs are composed of periodically positioned very small unit structures. MM theory is predicated on effective medium approach. Effective medium approach describes macroscopic features of a macroscopically homogeneous composite structures. These structures may not be necessarily homogenous in microscopic scale. However, the dimensions of the unit cells of the medium is required to be a small fraction of the free space wavelength i.e. at least one tenth of the wavelength [56,57].

After, referring the homogeneity, the **isotropy** of the medium is investigated here. An electromagnetically isotropic medium has the same electromagnetic properties towards every direction while an electromagnetic wave propagates. Since in an isotropic medium the primitive fields (**E** and **B**) and the induction fields (**D** and **H**) are co-directional, the constitutive dyadic/tensor terms reduce to scalar values [58] as indicated in Equations (2.7) and (2.8) of Tellegen representation. In such a case, the permittivity and permeability relations are given as:

$$\varepsilon = \varepsilon_0 \varepsilon_r \tag{2.18}$$

$$\mu = \mu_0 \mu_r \tag{2.19}$$

Free space (or vacuum) is linear and homogenous by definition. The permittivity and permeability parameters are defined only by $\varepsilon_0$ and $\mu_0$. The dielectric and magnetic substances are simple forms of media. In dissipative media permittivity and permeability are frequency dependent and they have complex values where the imaginary parts are positive.

In **anisotropic** media the primitive fields and induction fields are not co-directional contrary to isotropic media i.e. **D** is not aligned with **E** and/or **H** is not aligned with **B**. Unlike isotropic media, $\varepsilon$ and $\mu$ are identified in dyadic representation. The Tellegen constitutive relations of anisotropic homogenous media are specified as in Table 2.1.

**Table 2.1** Tellegen relations of anisotropic homogenous media

| ***Homogenous Media*** | ***Tellegen Relations*** | ***Eqn.*** |
|---|---|---|
| *Dielectric Medium* | $\mathbf{D} = \bar{\boldsymbol{\varepsilon}} \bullet \mathbf{E}$<br>$\mathbf{B} = \mu \mathbf{H}$ | (2.20) |
| *Magnetic Medium* | $\mathbf{D} = \varepsilon \bullet \mathbf{E}$<br>$\mathbf{B} = \bar{\boldsymbol{\mu}} \mathbf{H}$ | (2.21) |
| *Dielectric-Magnetic Medium* | $\mathbf{D} = \bar{\boldsymbol{\varepsilon}} \bullet \mathbf{E}$<br>$\mathbf{B} = \bar{\boldsymbol{\mu}} \mathbf{H}$ | (2.22) |

**Uniaxial** medium is defined by a distinguished axis at macroscopic scale and the axis may be specified by microscopic geometry and structure. For uniaxial dielectric medium the permittivity and permeability dyadic terms are identified by:

$$\bar{\boldsymbol{\varepsilon}}_{uni} = \begin{vmatrix} \varepsilon & 0 & 0 \\ 0 & \varepsilon & 0 \\ 0 & 0 & \varepsilon_u \end{vmatrix}, \qquad \bar{\boldsymbol{\mu}}_{uni} = \begin{vmatrix} \mu & 0 & 0 \\ 0 & \mu & 0 \\ 0 & 0 & \mu_u \end{vmatrix} \tag{2.23}$$

where *u* stands for the specified axis, in this case z-axis. Scalar elements of dyadic permittivity and permeability are set of complex numbers ($\varepsilon, \varepsilon_u, \mu, \mu_u \in \mathbb{C}$). For dissipative media the imaginary parts of elements of dyadic terms are positive.

The complex permittivity and permeability tensors for **biaxial** anisotropic homogenous media are tabulated and given in Table 2.2.

**Table 2.2** Dyadic terms of biaxial anisotropic homogenous media [58]

| *System* | *Dyadic Form* | *Dyadic Elements* |
|---|---|---|
| *Orthorhombic* | $\bar{\boldsymbol{\varepsilon}}_{bi} = \begin{vmatrix} \varepsilon_x & 0 & 0 \\ 0 & \varepsilon_y & 0 \\ 0 & 0 & \varepsilon_z \end{vmatrix}, \bar{\boldsymbol{\mu}}_{bi} = \begin{vmatrix} \mu_x & 0 & 0 \\ 0 & \mu_y & 0 \\ 0 & 0 & \mu_z \end{vmatrix}$ | $\varepsilon_x, \varepsilon_y, \varepsilon_z \in \mathbb{C}$<br>$\mu_x, \mu_y, \mu_z \in \mathbb{C}$ |
| *Monoclinic* | $\bar{\boldsymbol{\varepsilon}}_{bi} = \begin{vmatrix} \varepsilon_x & \varepsilon_a & 0 \\ \varepsilon_a & \varepsilon_y & 0 \\ 0 & 0 & \varepsilon_z \end{vmatrix}, \bar{\boldsymbol{\mu}}_{bi} = \begin{vmatrix} \mu_x & \mu_a & 0 \\ \mu_a & \mu_y & 0 \\ 0 & 0 & \mu_z \end{vmatrix}$ | $\varepsilon_x, \varepsilon_y, \varepsilon_z \in \mathbb{C}$<br>$\mu_x, \mu_y, \mu_z \in \mathbb{C}$<br>$\varepsilon_a, \mu_a \in \mathbb{R}$ |
| *Triclinic* | $\bar{\boldsymbol{\varepsilon}}_{bi} = \begin{vmatrix} \varepsilon_x & \varepsilon_a & \varepsilon_b \\ \varepsilon_a & \varepsilon_y & \varepsilon_c \\ \varepsilon_b & \varepsilon_c & \varepsilon_z \end{vmatrix}, \bar{\boldsymbol{\mu}}_{bi} = \begin{vmatrix} \mu_x & \mu_a & \mu_b \\ \mu_a & \mu_y & \mu_c \\ \mu_b & \mu_c & \mu_z \end{vmatrix}$ | $\varepsilon_x, \varepsilon_y, \varepsilon_z \in \mathbb{C}$<br>$\mu_x, \mu_y, \mu_z \in \mathbb{C}$<br>$\varepsilon_a, \varepsilon_b, \varepsilon_c \in \mathbb{R}$<br>$\mu_a, \mu_b, \mu_c \in \mathbb{R}$ |

**Bianisotropy** keeps an important place in MM field due to its exotic features such as asymmetric reflection [34]. The bianisotropic MMs have different forward and backward wave impedances and wider stopband in transmission [26]. Bianisotropy of a medium is due to magnetoelectric coupling. Hence, in a bianisotropic medium electric and magnetic flux densities, **D** and **B** include both electric and magnetic field intensities, **E** and **H**, in Tellegen relations. The relations for a homogenous bianisotropic medium may be given as:

$$\mathbf{D} = \bar{\boldsymbol{\varepsilon}} \bullet \mathbf{E} + \bar{\boldsymbol{\varsigma}} \bullet \mathbf{H} \tag{2.24}$$

$$\mathbf{B} = \bar{\boldsymbol{\mu}} \bullet \mathbf{H} + \bar{\boldsymbol{\zeta}} \bullet \mathbf{E} \tag{2.25}$$

The constitutive parameters of bianisotropic media are represented by 3 by 3 dyadic terms, in general. Complex permittivity, permeability and transversal coupling tensors are given in Table 2.3.

**Table 2.3** Dyadic terms for bianisotropic media

| ***Name*** | ***Dyadic Form*** | ***Dyadic Elements*** |
|---|---|---|
| *Complex constitutive tensors* | $\bar{\boldsymbol{\varepsilon}} = \begin{vmatrix} \varepsilon_x & \varepsilon_a & \varepsilon_b \\ \varepsilon_a & \varepsilon_y & \varepsilon_c \\ \varepsilon_b & \varepsilon_c & \varepsilon_z \end{vmatrix}, \bar{\boldsymbol{\mu}} = \begin{vmatrix} \mu_x & \mu_a & \mu_b \\ \mu_a & \mu_y & \mu_c \\ \mu_b & \mu_c & \mu_z \end{vmatrix}$ | $\varepsilon_x, \varepsilon_y, \varepsilon_z \in \mathbb{C}$ <br> $\mu_x, \mu_y, \mu_z \in \mathbb{C}$ <br> $\varepsilon_a, \varepsilon_b, \varepsilon_c \in \mathbb{R}$ <br> $\mu_a, \mu_b, \mu_c \in \mathbb{R}$ |
| *Transversal coupling tensors* | $\bar{\boldsymbol{\varsigma}} = \begin{vmatrix} \varsigma_x & \varsigma_a & \varsigma_b \\ \varsigma_a & \varsigma_y & \varsigma_c \\ \varsigma_b & \varsigma_c & \varsigma_z \end{vmatrix}, \bar{\boldsymbol{\zeta}} = \begin{vmatrix} \zeta_x & \zeta_a & \zeta_b \\ \zeta_a & \zeta_y & \zeta_c \\ \zeta_b & \zeta_c & \zeta_z \end{vmatrix}$ | $\varsigma_x, \varsigma_y, \varsigma_z \in \mathbb{C}$ <br> $\zeta_x, \zeta_y, \zeta_z \in \mathbb{C}$ <br> $\varsigma_a, \varsigma_b, \varsigma_c \in \mathbb{R}$ <br> $\zeta_a, \zeta_b, \zeta_c \in \mathbb{R}$ |

For **orthorhombic biaxial bianisotropic** medium, the following terms are zero.

$$\begin{aligned} \varepsilon_a &= \varepsilon_b = \varepsilon_c = 0 \\ \mu_a &= \mu_b = \mu_c = 0 \\ \varsigma_a &= \varsigma_b = \varsigma_c = 0 \\ \zeta_a &= \zeta_b = \zeta_c = 0 \end{aligned} \tag{2.26}$$

Also, for **uniaxial bianisotropic** medium, the following terms are set as specified, in addition to terms given in Equation (2.26).

$$\begin{aligned} \varepsilon_x &= \varepsilon_y \\ \mu_x &= \mu_y \\ \varsigma_x &= \varsigma_y \\ \zeta_x &= \zeta_y \end{aligned} \tag{2.27}$$

## 2.6 Problem Description

Electric magnetic field intensities **E** and **H** are coupled together within a biaxial bianisotropic sample with specified $e_1 \parallel \hat{a}_x$, $e_2 \parallel -\hat{a}_z$ and $e_3 \parallel \hat{a}_y$ axes due to the electric and magnetic excitation. The Tellegen relation for the biaxial bianisotropic sample was submitted in Equations (2.24) and (2.25). The complex constitutive permittivity, permeability and transversal coupling dyadic parameters of the bianisotropic material may be identified as:

$$\bar{\boldsymbol{\varepsilon}} = \varepsilon_0 \begin{vmatrix} \varepsilon_1 & 0 & 0 \\ 0 & \varepsilon_3 & 0 \\ 0 & 0 & \varepsilon_2 \end{vmatrix}, \quad \bar{\boldsymbol{\mu}} = \mu_0 \begin{vmatrix} \mu_1 & 0 & 0 \\ 0 & \mu_3 & 0 \\ 0 & 0 & \mu_2 \end{vmatrix} \tag{2.28}$$

$$\bar{\boldsymbol{\varsigma}} = \frac{1}{c} \begin{vmatrix} 0 & 0 & 0 \\ -i\xi_0 & 0 & 0 \\ 0 & 0 & 0 \end{vmatrix}, \quad \bar{\boldsymbol{\zeta}} = \frac{1}{c} \begin{vmatrix} 0 & i\xi_0 & 0 \\ 0 & 0 & 0 \\ 0 & 0 & 0 \end{vmatrix} \tag{2.29}$$

In above equations, c and $\xi_0$ indicate the speed of light in vacuum and magneto-electric coupling value. In addition, $\varepsilon_1\,(\mu_1)$, $\varepsilon_3\,(\mu_3)$ and $\varepsilon_2\,(\mu_2)$ are complex permittivity (permeability) elements. The main goal of this study is to retrieve $\varepsilon_3$, $\mu_1$, $\mu_2$ and $\xi_0$ parameters [59]. It is assumed that the electromagnetic wave propagates towards *z*-axis, electric and magnetic excitations ($E_y$, $H_x$) are in *y* and *x* directions, respectively.

Bi-axial bianisotropic MM samples can be characterized via waveguide measurements in microwave region. Generally, in waveguide characterization measurements, it is supposed that the reference plane is overlapped with the measurement plane of specimen. However, the problem to be investigated is to perform the measurements accurately, without knowledge of position of an arbitrarily placed slab into the measurement setup. In order to extract constitutive electromagnetic properties correctly, the retrieval algorithm must be specified elaborately. For that reason, a waveguide measurement setup with an arbitrarily inserted specimen inside of it should be investigated. The situation is illustrated in Figure 2.9.

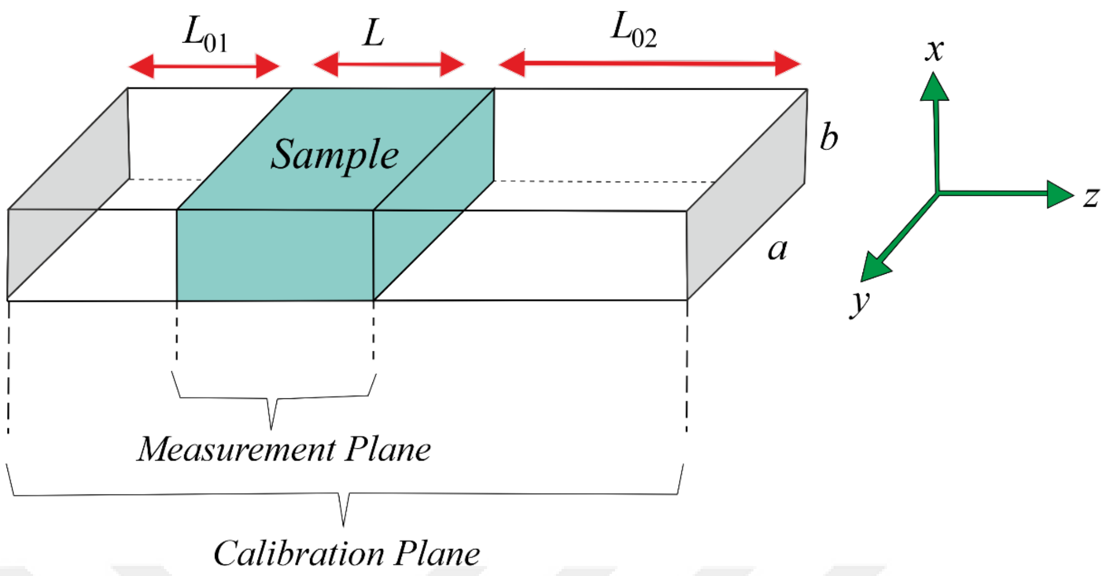


**Figure 2.9** Arbitrarily inserted biaxial sample with length L into a waveguide frame with distances $L_{01}$ and $L_{02}$ between measurement and calibration planes

In the given illustration, a biaxial sample with a length *L* is positioned into metallic hollow waveguide structure with transversal dimensions *a* and *b*. In this problem, it is supposed that the calibration is performed to given calibration planes. As it seen, the calibration planes are not overlapped with the measurement planes of the sample. There are gaps between calibration planes and measurement planes and they are denoted by $L_{01}$ and $L_{02}$.

The propagation of electromagnetic wave through the measured slab inside the waveguide is in the *z*-axis and the longitudinal components of primitive fields **E**z and **H**z are generally coupled together. It is described that; this electromagnetic coupling is spoiled if both of **E**z and **H**z components are not varying over the *xy*-plane [61]. In the described problem, the dominant mode $\mathrm{TE}_{10}^{z}\left(\partial/\partial y=0\right)$ propagates through the waveguide frame whose cross-section is entirely filled by the biaxial sample, noting that only $\mathrm{TE}_{m0}^{z}$ varying with *x* and *z* axis will be able to propagate through the biaxial specimen where m indicates half sinusoidal variation in *x*-axis. In addition, assuming the calibration and measurement planes are placed far away then higher order modes will be neglectable.

For $e^{-i\omega t}$ convention, S-parameters at the calibration planes of experimental setup of the biaxial bianisotropic MM sample may be given as:

$$S_{11} = R_{01}^2 \left[ \frac{\Gamma_1 \left(1 - \mathrm{T}^2\right)}{1 - \Gamma_1 \Gamma_2 \mathrm{T}^2} \right] \tag{2.30}$$

$$S_{22} = R_{02}^2 \left[ \frac{\Gamma_2 \left(1 - \mathrm{T}^2\right)}{1 - \Gamma_1 \Gamma_2 \mathrm{T}^2} \right] \tag{2.31}$$

$$S_{21} = S_{12} = R_{01} R_{02} \left[ \frac{\mathrm{T}\left(1 - \Gamma_1 \Gamma_2\right)}{1 - \Gamma_1 \Gamma_2 \mathrm{T}^2} \right] \tag{2.32}$$

where $\Gamma_1$, $\Gamma_2$ and $\mathrm{T}$ are semi-infinite reflection coefficients and propagation factor, respectively. The propagation factor is:

$$\mathrm{T} = e^{i\beta_{sz} L} \tag{2.33}$$

Furthermore, the normalized forward and backward wave impedances ( $z_{ws}^+$, $z_{ws}^-$ ) and phase constant ( $\beta_{sz}$ ) towards *z*-axis within the biaxial bianisotropic sample may be given as:

$$z_{ws}^+ = \frac{1 + \Gamma_1}{1 - \Gamma_1} = \frac{\mu_1 \beta_{0z}}{\beta_{sz} + i k_0 \xi_0} \tag{2.34}$$

$$z_{ws}^- = \frac{1 + \Gamma_2}{1 - \Gamma_2} = \frac{\mu_1 \beta_{0z}}{\beta_{sz} - i k_0 \xi_0} \tag{2.35}$$

$$\beta_{sz} = \sqrt{k_0^2 \left( \varepsilon_3 \mu_1 - \xi_0^2 \right) - \frac{\mu_1}{\mu_2} \beta_{0x}^2} \tag{2.36}$$

$k_0 = \omega / c$ is the phase constant in unbounded air where $\omega$ is the angular frequency of the propagating wave. Also, $\beta_{0x}$, $\beta_{0z}$ are phase constants towards *x* and *z* axes within the air region of the waveguide and may be given as:

$$\beta_{0x} = \frac{\pi}{a} \tag{2.37}$$

$$\beta_{0z} = \sqrt{k_0^2 - \beta_{0x}^2} \tag{2.38}$$

Finally, $R_{01}$ and $R_{02}$ may be given as:

$$R_{01} = e^{i\beta_{0z}L_{01}} \tag{2.39}$$

$$R_{02} = e^{i\beta_{0z}L_{02}} \tag{2.40}$$

It is noted that, the tensors given in the Equations (2.28) and (2.29) fulfil the reciprocity conditions such that: $\overline{\boldsymbol{\varepsilon}}^T = \overline{\boldsymbol{\varepsilon}}$, $\overline{\boldsymbol{\mu}}^T = \overline{\boldsymbol{\mu}}$ and $\overline{\boldsymbol{\zeta}}^T = -\overline{\boldsymbol{\zeta}}$ thus, demonstrating that the biaxial bianisotropic MM sample under the investigation is reciprocal i.e. ideally S-parameters are $S_{21} = S_{12}$ [26].

## 2.7 Proposed Reference-Plane-Invariant Methodology

As it seen through the Equations (2.28) and (2.40), the constitutive parameters $\varepsilon_3$, $\mu_1$, $\mu_2$ and $\xi_0$ are functions of distances between calibration and measurement planes, $L_{01}$ and $L_{02}$ through the S-parameters. Thus, in order to extract the aforesaid constitutive parameters, precise knowledge of $L_{01}$ and $L_{02}$ values are necessary. For the purpose of extraction of these parameters without requiring the reference plane information, the following constitutive parameters retrieval technique is proposed [60]. We begin with the following relations to the proposed technique [38,39,41,60]:

$$A = \frac{S_{11}S_{22}}{S_{21}S_{12}} = \frac{\Gamma_1\Gamma_2\left(1-\mathrm{T}^2\right)^2}{\mathrm{T}^2\left(1-\Gamma_1\Gamma_2\right)^2} \tag{2.41}$$

$$B = \frac{S_{21}}{S_{21}^{(0)}} = \frac{1}{R_0}\frac{\mathrm{T}\left(1-\Gamma_1\Gamma_2\right)}{\left(1-\Gamma_1\Gamma_2\mathrm{T}^2\right)} \tag{2.42}$$

where $S_{21}^{(0)}$ is the transmission S-parameter for the empty cell. Similarly, $R_0$ is defined as:

$$R_0 = e^{i\beta_{0z}L} \tag{2.43}$$

In the above-defined equations, $A$ and $B$ are not functions of $R_{01}$ and $R_{02}$ parameters as can be seen. The complex exponential transmission term T should be eliminated from the Equations (2.41) and (2.42) since it produces multiple solutions. Thus, $\mathrm{T}^2$ term is calculated as:

$$\mathrm{T}^2 = \frac{1+\chi}{(1-\chi)/\left(R_0^2 B^2\right) + \chi\left[2 - A(1-\chi)\right]} \tag{2.44}$$

where $\chi = \Gamma_1 \Gamma_2$. And then, inserting $\mathrm{T}^2$ term into the Equation (2.41), we can obtain:

$$\chi^2 + \left[(2-A)R_0^2 B^2 - \frac{\left(1 - R_0^2 B^2\right)^2}{A R_0^2 B^2}\right]\chi + 1 = 0 \tag{2.45}$$

The reflection terms $\Gamma_1$ and $\Gamma_2$ could be obtained by finding magnitude and then phase angle, subsequently. Thus, reflection terms may be written in phasor notation as:

$$\Gamma_1 = \left|\Gamma_1\right| e^{i\theta_1} \tag{2.46}$$

$$\Gamma_2 = \left|\Gamma_2\right| e^{i\theta_2} \tag{2.47}$$

To obtain magnitudes of reflection terms, S-parameter expressions $S_{11}$ and $S_{22}$ are used since the reflection terms are in product form. The $S_{11}$ and $S_{22}$ may be re-written as:

$$\left|S_{11}\right| = \left|\frac{\Gamma_1\left(1 - \mathrm{T}^2\right)}{1 - \chi \mathrm{T}^2}\right| \tag{2.48}$$

$$|S_{22}| = \left| \frac{\chi(1-\mathrm{T}^2)}{\Gamma_1(1-\chi\mathrm{T}^2)} \right| \tag{2.49}$$

Thus, the magnitude reflection terms can be retrieved by using the following relations:

$$|\Gamma_1| = \sqrt{\frac{|S_{11}|}{|S_{22}|}|\chi|}, \qquad |\Gamma_2| = \frac{|\chi|}{|\Gamma_1|} \tag{2.50}$$

Thereafter, for determining angles of phasors, $\theta_1$ and $\theta_2$, again the $S_{11}$ and $S_{22}$ parameters are used. Using the following relations $\theta_1$ and $\theta_2$ will be obtained in terms of $L_{01}$ and $L_{02}$ distance parameters, respectively.

$$R_1^2 e^{i\theta_1} = S_{11} \frac{1-\chi\mathrm{T}^2}{|\Gamma_1|(1-\mathrm{T}^2)} = |M| e^{i\theta_M} \tag{2.51}$$

$$R_2^2 e^{i\theta_2} = S_{22} \frac{1-\chi\mathrm{T}^2}{|\Gamma_2|(1-\mathrm{T}^2)} = |N| e^{i\theta_N} \tag{2.52}$$

$$\theta_1 = \theta_M - 2L_{01}\beta_{0z}, \qquad \theta_2 = \theta_N - 2L_{02}\beta_{0z} \tag{2.53}$$

As can be seen in Equations (2.51) – (2.53), if $L_{01}$ and $L_{02}$ values could be obtained, then $e^{i\theta_1}$ and $e^{i\theta_2}$ terms can be calculated. Now, the problem turns into retrieval of $L_{01}$ and $L_{02}$ parameters. In order to solve this problem, the varying-frequency technique [62,63] is utilized here. By employing this technique, a $\theta$ angle may be written by utilizing two of neighboring frequencies such that:

$$f_2 = f_1 \pm \Delta f \quad \text{where} \quad \Delta f \ll f_1 \tag{2.54}$$

Then, after assuming the reflection terms are almost same for the neighboring frequencies, i.e. $\Gamma_1(f_1) \cong \Gamma_1(f_2)$, the relation for $\theta_1$ may be expressed as:

$$\theta_1(f_1) = \theta_M(f_1) - 2L_{01}\sqrt{\left(\frac{2\pi f_1}{c}\right)^2 - \beta_{0x}^2} \tag{2.55}$$

$$\theta_1(f_2) = \theta_M(f_2) - 2L_{01}\sqrt{\left(\frac{2\pi f_2}{c}\right)^2 - \beta_{0x}^2} \tag{2.56}$$

Towards this end, using the relations given in the Equations (2.51) – (2.56), the distance parameter $L_{01}$ between calibration and measurement plane can be calculated as given in the following equation.

$$L_{01} = \frac{\theta_M(f_1) - \theta_M(f_2)}{2\left[\sqrt{\left(\frac{2\pi f_1}{c}\right)^2 - \beta_{0x}^2} - \sqrt{\left(\frac{2\pi f_2}{c}\right)^2 - \beta_{0x}^2}\right]} \tag{2.57}$$

After calculating $L_{01}$ by using relation given in Equation (2.57), $e^{i\theta_1}$ could be directly calculated by using Equation (2.51). Later on, reflection term $\Gamma_2$ is calculated via $\chi$ which appears in the Equation (2.45). In case of the condition $\Gamma_1(f_1) \cong \Gamma_1(f_2)$ does not hold, this approach can be applied to the second reflection term as, $\Gamma_2(f_1) \cong \Gamma_2(f_2)$. Similarly, the relation for $L_{02}$ may be given as:

$$L_{02} = \frac{\theta_N(f_1) - \theta_N(f_2)}{2\left[\sqrt{\left(\frac{2\pi f_1}{c}\right)^2 - \beta_{0x}^2} - \sqrt{\left(\frac{2\pi f_2}{c}\right)^2 - \beta_{0x}^2}\right]} \tag{2.58}$$

Again, similarly $e^{i\theta_2}$ is calculated via $\chi$ which appears in the Equation (2.45). $L_{01}$ and $L_{02}$ are dimensional parameters, they can be obtained for any frequency interval, however, the constitutive parameters that are calculated by using dimensional parameters will be valid over entire frequency interval.

Before, giving the final relations in order to calculate constitutive parameters, the relation for transmission term T is given as:

$$\mathrm{T}=\frac{BR_0\left(1-\chi\mathrm{T}^2\right)}{1-\chi} \tag{2.59}$$

At the end, after describing the Equation (2.59), the aforementioned complex constitutive parameters can be calculated by using Equations (2.34) – (2.36) and may be given as:

$$\xi_0=\frac{\beta_{sz}\left(\Gamma_2-\Gamma_1\right)}{ik_0\left(1-\chi\right)} \tag{2.60}$$

$$\mu_1=\frac{\left(\beta_{sz}+ik_0\xi_0\right)}{\beta_{0z}}\frac{\left(1+\Gamma_1\right)}{\left(1-\Gamma_1\right)} \tag{2.61}$$

$$\varepsilon_3=\frac{1}{\mu_1}\left(\frac{\beta_{sz}^2+\mu_1\beta_{0x}^2}{k_0^2}+\xi_0^2\right) \tag{2.62}$$

$$\beta_{sz}=\frac{\ln\left(\mathrm{T}\right)\pm i2\pi m}{iL} \tag{2.63}$$

where m is a natural number. Also, it is supposed that permeability parameter in *z*-direction $\mu_2=1$ [33,34,64,65] and it was validated through the experimental studies [36,34].

## 2.8 De-embedding Technique

Sometimes the sample to be measured are composed of multiple layers and the electromagnetic parameters of a specific layer may be desired. In such a case, the effects of additional layers should be removed. For this purpose, de-embedding technique may be utilized. Let's assume a sample composing of X, Y and Z layers and it is not possible to measure electromagnetic properties of Y-layer only. If ABCD matrices of X and Z layers are measurable separately or known, their effects can be eliminated by the de-embedding technique.

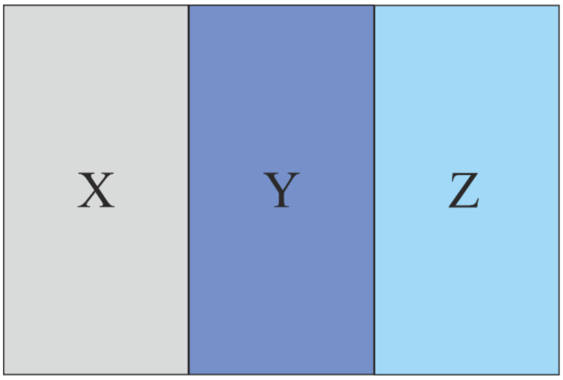


**Figure 2.10** A sample consisting of three different layers through wave propagation direction

The overall ABCD matrix of the multilayered sample may be written in terms of ABCD matrices of sublayers as:

$$T_{XYZ} = T_X T_Y T_Z \tag{2.64}$$

In order to de-embed the layers X and Z, and obtain ABCD matrix of Y-layer, the following relation may be used.

$$T_Y = T_X^{-1} T_{XYZ} T_Z^{-1} \tag{2.65}$$

An ABCD matrix may be written as:

$$T = \begin{bmatrix} A & B \\ C & D \end{bmatrix} \tag{2.66}$$

where the elements of ABCD matrix are:

$$A = \frac{(1+S_{11})(1-S_{22}) + S_{21}S_{12}}{2S_{21}} \tag{2.67}$$

$$B = \frac{(1+S_{11})(1+S_{22}) - S_{21}S_{12}}{2S_{21}} \tag{2.68}$$

$$C = \frac{(1-S_{11})(1-S_{22}) - S_{21}S_{12}}{2S_{21}} \tag{2.69}$$

$$D = \frac{(1-S_{11})(1+S_{22}) + S_{21}S_{12}}{2S_{21}} \tag{2.70}$$

After the de-embedding, the S-parameters of the layer could be retrieved back from the calculated ABCD matrix as:

$$S_{11} = \frac{A+B-C-D}{A+B+C+D} \tag{2.71}$$

$$S_{12} = \frac{2(AD-BC)}{A+B+C+D} \tag{2.72}$$

$$S_{21} = \frac{2}{A+B+C+D} \tag{2.73}$$

$$S_{22} = \frac{-A+B-C+D}{A+B+C+D} \tag{2.74}$$

# CHAPTER 3

# RESULTS AND DISCUSSION

In this chapter, the structural and geometrical parameters of the designed biaxial bianisotropic MM are given. 3D electromagnetic simulation environment and the results for the designed MM structure are reported. Subsequently, measurement experiments of the fabricated MM structure and the measurement results are provided. The comments about the obtained results are presented.

## 3.1 Design of Biaxial Bianisotropic MM Structure

For this study, a MM unit cell that consists of square shaped SRR with one split, is considered to be used. The designed unit cell has only one ring instead of having another additional coaxial inner ring due to facilitating fabrication process of the MM structure. In order to satisfy the effective medium approach, an approximately homogenous medium, the SRR structures must be very small in dimension. As the dimensions are getting smaller, the fabrication of metallic SRR structures become difficult and expensive. Although it is possible to produce SRRs in nanometric scale with sophisticated production techniques, unfortunately, the production costs reach to extreme levels.

The MM unit cell is composed of a metallic SRR structure and two layers of dielectric substance. The SRR inclusion is tightly sandwiched between the two dielectric (FR4) substrates to form a symmetric pattern in $x$-direction. The unit cell is illustrated in Figure 3.1 in cross-sectional perspective and accordingly, the structural properties and geometrical parameters are provided in Table 3.1.

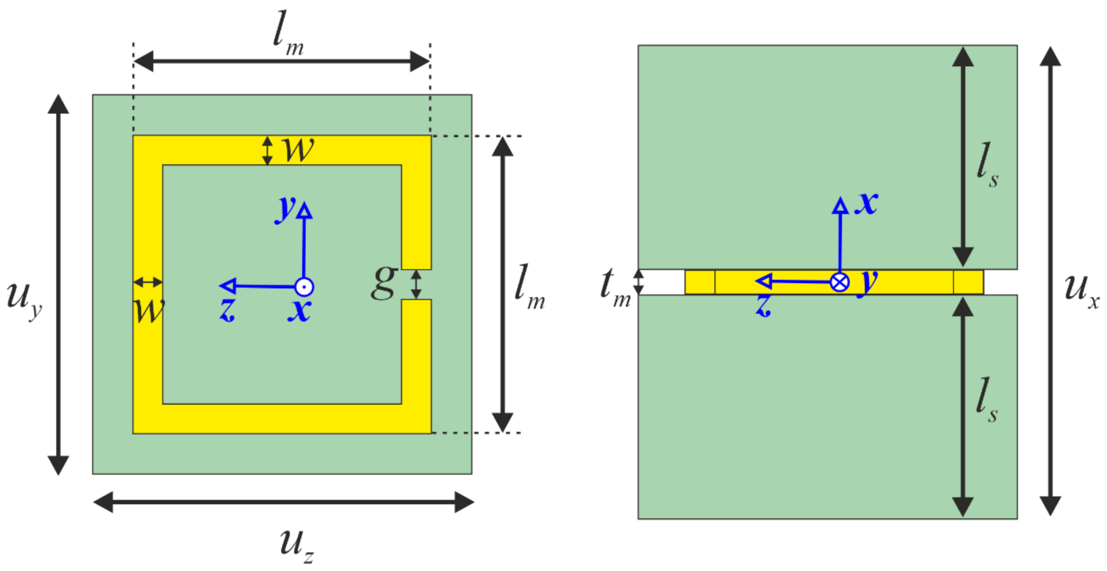


**Figure 3.1** Cross-sectional front and side views of the designed MM unit cell

**Table 3.1** Structural and geometrical parameters of the MM unit cell

| Explanation | Symbol and Value | Unit |
|---|---|---|
| Dielectric substrate thickness (FR4 material) | $l_s = 1.5$ | mm |
| Dielectric constant of the substrate | $\varepsilon_d = 4.3$ | - |
| Loss tangent of the substrate | $\tan\delta_d = 0.025$ | - |
| Metallization length of the SRR (Copper) | $l_m = 2$ | mm |
| Metallization thickness of the SRR | $t_m = 35$ | µm |
| Conductivity of the SRR | $\sigma_c = 5.8\times10^7$ | S/m |
| Metallization width of the SRR | $w = 0.3$ | mm |
| Length of split of the SRR | $g = 0.3$ | mm |
| Length of unit cell along $x$-direction | $u_x = 2l_s + t_m$ | mm |
| Length of unit cell along $y$-direction | $u_y = 2.54$ | mm |
| Length of unit cell along $z$-direction | $u_z = 2.54$ | mm |

It is supposed that the three coordinate axes of the unit cell of the MM, $e_1$, $e_2$ and $e_3$ are aligned with the $x$, $-z$ and $y$ directions, respectively which is shown in Figure 3.2.

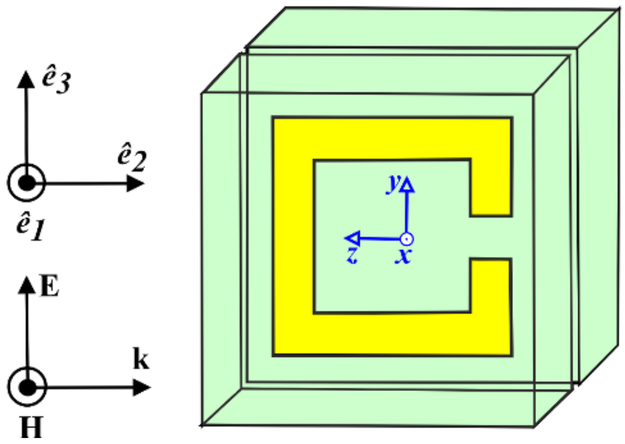


**Figure 3.2** Geometry and axes of MM unit cell and incident electromagnetic wave

The MM unit cell is adjusted to fill the entire cross-sectional frame of an X-band waveguide (the frequency range is between $f_1$=8.2 GHz and $f_2$=12.4 GHz and the cut off frequency is $f_c$=6.557 GHz for an X-band waveguides) which has transversal dimensions of $a = 22.86$ mm and $b = 10.16$ mm. As illustrated in Figure 3.3, a column of the MM slab is composed of four MM unit cells in $y$-direction. Also, it is possible to be inserted seven columns at maximum in $x$-direction. For the purpose of completing the MM structure in the waveguide frame, the tiny vacancy remained in the $x$-direction is filled with two thin identical FR4 substrates at the either sides of the MM structure.

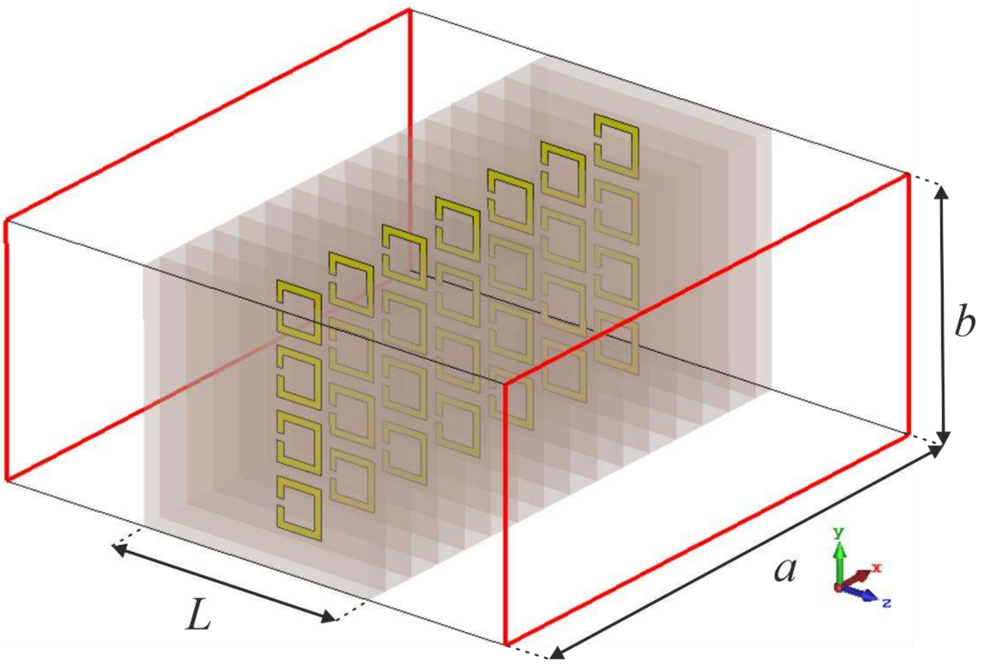


**Figure 3.3** Illustration of the constructed MM slab inside X-band waveguide frame

The overall slab of MM structure has the periodicity of $u_x \cong 3$ mm and $u_y = 2.54$ mm in *x* and *y* directions and thus, the periodicity is much less than free space wavelength $\lambda = 30$ mm, to satisfy effective medium approach.

As it is described in Section 2.6, the dominant mode ($\mathrm{TE}_{10}^{z}$) propagates inside the waveguide throughout the MM sample. For this dominant mode, the magnetic field component of the propagating wave is perpendicular to the SRR plane which induces circulating and oscillating current in the metallic ring producing a magnetic dipole in *x*-direction. Next, the electric field perpendicular to the slit of the SRR will produce electric dipole in *y*-direction due to the accumulation of charges of opposite polarities at edges and corners of the SRR. In addition, the electric and magnetic fields couple with each other, such that the magnetic dipole and electric dipole is generated (in *x* and *y* directions, respectively) by the excitation of electric and magnetic fields, respectively [60,66]. Due to this cross excitation, the MM gains bianisotropic property (asymmetric reflection).

### 3.2 Validation of the Proposed Method via Numerical Simulations

In order to validate the proposed method, first numerical simulations were conducted for the designed MM structure. A commercial 3D electromagnetic analysis software, CST Microwave Studio, which is based on finite integration technique is used for the simulation throughout the study. To simulate metallic waveguide frame, perfect electric conductor (PEC) boundary conditions are applied to the boundaries of the designed MM structure (having dimensions of X-band waveguides), at $x = \pm a/2$ and $y = \pm b/2$ planes. In CST Microwave Studio user interface, the PEC boundary condition is applied by selecting “Electric (Et=0)” option. Thanks to the PEC boundary conditions by the mirror imaging effect, the periodicity is continued beyond the prepared MM slab, along *x* and *y* axes.

Additionally, open boundaries are applied at planes of the MM structure and input and output ports are located perpendicular to wave propagation vector **k**, along *z*-axis. As specified in Section 2.6, the distances between input port – MM surface and MM surface – output port are identified by $L_{01}$ and $L_{02}$ parameters. In order to implement necessary minimum mesh number to obtain accurate the simulation results, the adaptive mesh refinement feature of the software is utilized.

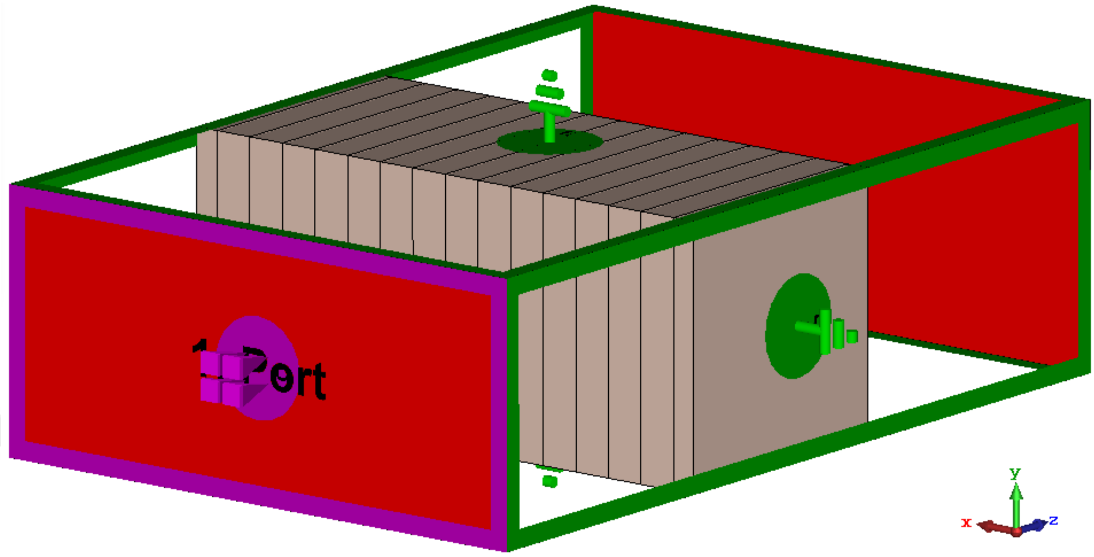


**Figure 3.4** Simulation layout for the prepared bianisotropic MM sample with the assigned PEC boundary conditions and input-output ports

It should be noted that, length of MM slab $L$=10.16 mm in z-direction, should have been equal to the length of unit cell $u_z = 2.54$ mm. However, it is constructed with L=10.16 mm to ease the measurements and to reduce effects of dimensional uncertainties in the wave propagation direction. The effect of complementary FR4 substrates on left and right sides of the MM slab in z-direction will be removed by utilizing de-embedding technique [67].

Two different types of simulations are performed to investigate the precision of the proposed method and it is compared with a proposed reference-plane-dependent (RPD) method [34]. In first type of simulations, the length parameters $L_{01}$ and $L_{02}$ were set to zero i.e. the calibration and measurement planes are overlapped, and then $\chi$ was calculated by using Equation (2.45) and $|\Gamma_1|$, $|\Gamma_2|$ were calculated by using Equation (2.50) for the bianisotropic MM sample. The dependencies of $\chi$, $|\Gamma_1|$ and $|\Gamma_2|$ obtained by the first type simulation ($L_{01}$= $L_{02}$=0) are plotted for X-band, as given in Figure 3.5.

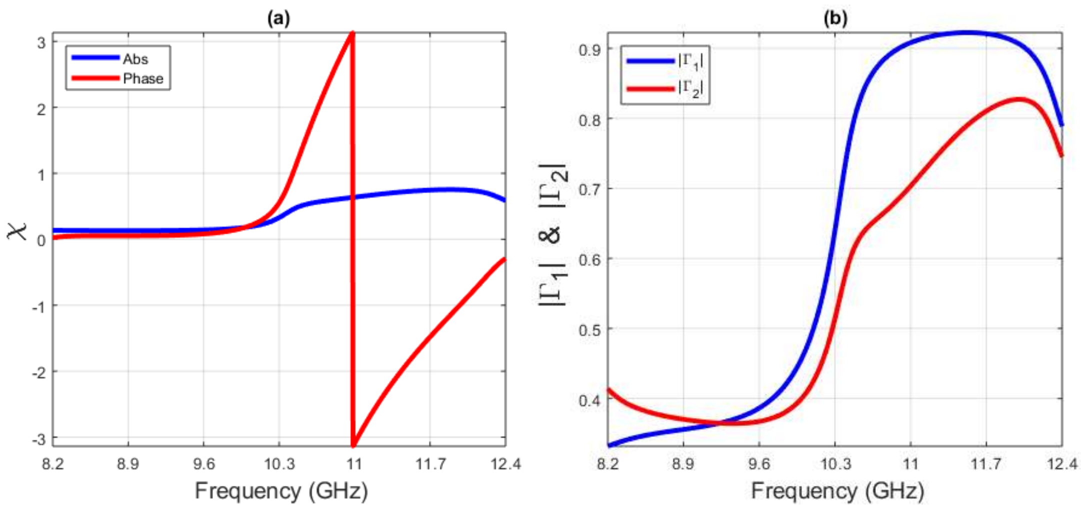


**Figure 3.5** $\chi$, $|\Gamma_1|$ and $|\Gamma_2|$ dependencies of the bianisotropic MM slab with length $L$=10.16 mm by the proposed RPI method using S-parameters ($L_{01}$=$L_{02}$=0)

Next, $e^{i\theta_1}$ and $e^{i\theta_2}$ are calculated by utilizing the frequency-varying technique. With the technique, a frequency range must be selected such that $\chi$ and $|\Gamma|$ parameters have small variation, for a better calculation. Thus, as a first step, the frequency range 8.7 GHz to 9.7 GHz is selected and, in this range, $\chi$ and $|\Gamma|$s slightly vary as it is noted in Figure 3.5 (a) and (b). Secondly, frequency step size $\Delta f = |f_1 - f_2|$ is assigned large enough to produce separate $M$ and $N$ values and thus, $\Delta f = 100$ MHz is assigned. Thirdly, any $f_1$ is selected ($f_1 = 8.8$ GHz, here) in the range and then $e^{i\theta_1}$ and $e^{i\theta_2}$ are calculated after calculating $L_{01}$ and $L_{02}$ by using the Equations (2.57) and (2.58) for the assigned frequency step size. Fourthly, the calculation of $e^{i\theta_1}$ and $e^{i\theta_2}$ is continued by reducing $\Delta f$ parameter until converging $e^{i\theta_1}$ and $e^{i\theta_2}$ values. Finally, the same process is repeated for new selected frequencies (in the specified range) to check consistency of the calculated $e^{i\theta_1}$ and $e^{i\theta_2}$ values. These mentioned steps are applied for both $L_{01}$ and $L_{02}$ and the best results were obtained from the $L_{02}$ determination with the calculated values of $L_{01}$ = 0.0543 mm and $L_{02}$ = - $L_{01}$.

After obtaining $L_{01}$ and $L_{02}$, the calculation of $e^{i\theta_1}$ and $e^{i\theta_2}$ is performed by using Equations (2.51) and (2.51), and $R_{01}$ and $R_{02}$ is performed by the Equations (2.39) and

(2.40). In addition, reference-plane independent S-parameters are calculated from Equations (2.30) - (2.32) as follows.

$$S_{11}^{RPI} = \frac{S_{11}}{R_{01}^2} \tag{3.1}$$

$$S_{22}^{RPI} = \frac{S_{22}}{R_{02}^2} \tag{3.2}$$

$$S_{21}^{RPI} = \frac{S_{21}}{R_{01}R_{02}}, \; S_{12}^{RPI} = \frac{S_{12}}{R_{01}R_{02}} \tag{3.3}$$

After all these calculations, the de-embedding technique [67] is applied to the produced MM slab having $L$ = 10.16 mm to obtain constitutive parameters of the designed MM slab with length $L = u_z$ = 2.54 mm (Figure 3.2). By this method, the effects of extra FR4 materials at the leading and trailing edges of the constructed MM slab will be eliminated. In order to apply the de-embedding method, ABCD matrix of the entire bianisotropic MM slab with length $L$ = 10.16 mm ($T_{\text{entire}}$) was obtained first by using $S_{11}^{RPI}$, $S_{21}^{RPI}$, $S_{12}^{RPI}$ and $S_{22}^{RPI}$ parameters. Subsequently, the entire MM slab along $z$-axis is assumed to be separated into three individual regions, FR4 dielectric materials at the leftmost and rightmost sides and MM unit cell at the middle. The ABCD matrices of the FR4 substrates ($T_{FR4}^{L}$ and $T_{FR4}^{R}$) at the left and right edges having lengths of;

$$L_{FR4}^{L} = L_{FR4}^{R} = \frac{L - u_z}{2} = 3.81 \text{ mm} \tag{3.4}$$

are calculated using the material properties of FR4, permittivity value $\varepsilon_d = 4.3$ and loss tangent value $\tan\delta_d = 0.025$. Finally, the ABCD matrix of the MM unit cell is calculated to be:

$$T_{UC} = \left(T_{FR4}^{L}\right)^{-1} T_{entire} \left(T_{FR4}^{R}\right)^{-1} \tag{3.5}$$

Thus, the S-parameters of the MM unit cell with length $L = u_z = 2.54$ mm is obtained via the calculated ABCD matrix given just above. In the end, the effective constitutive parameters $\beta_{sz}, \varepsilon_3, \mu_1$ and $\xi_0$ of the bianisotropic MM slab with $L$ = 2.54 mm are retrieved by using RPI method with the parameters set to $L_{01} = L_{02} = 0$. The plots for parameters are presented in Figures 3.6 and 3.7.

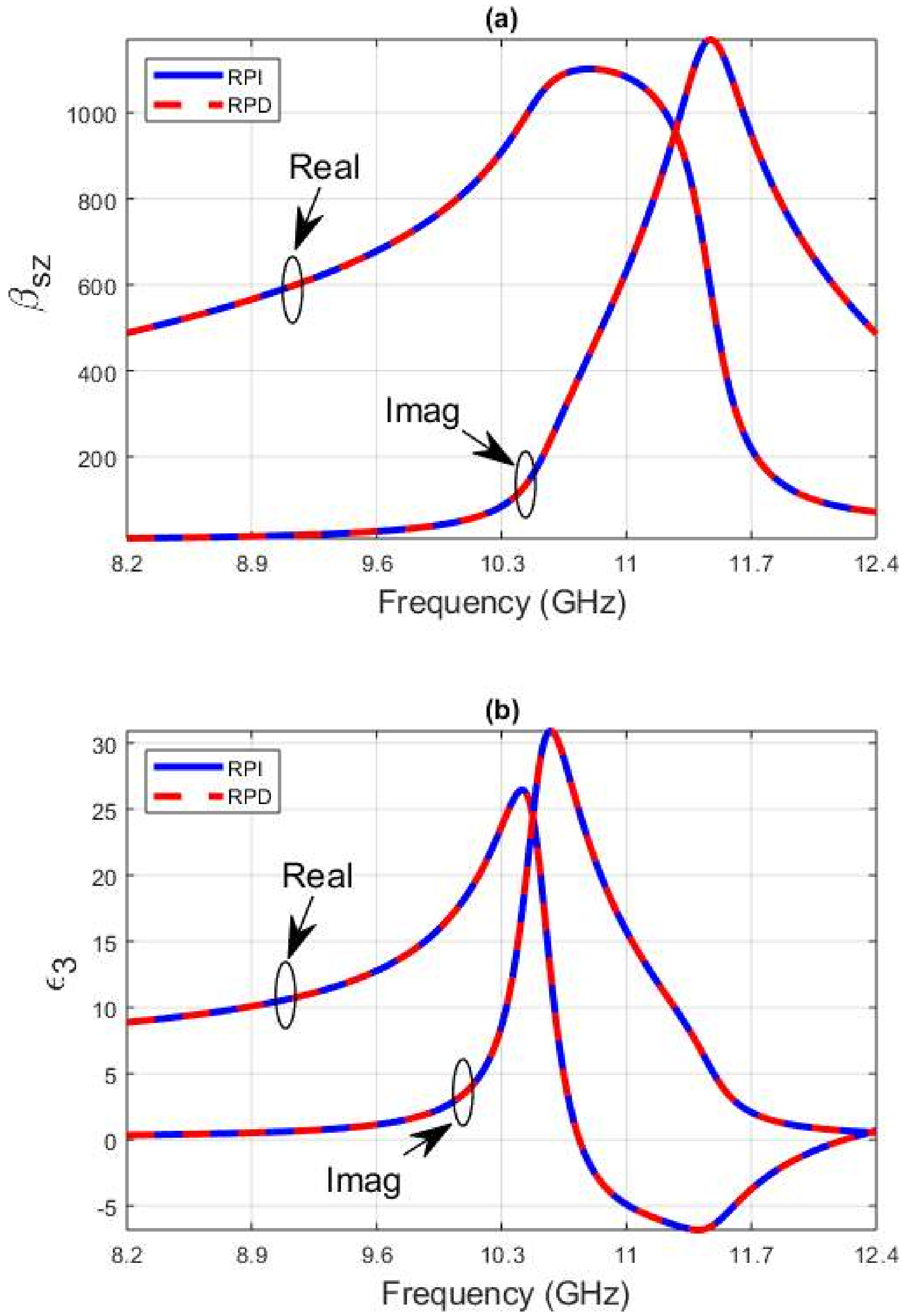


**Figure 3.6** Extracted $\beta_{sz}$ and $\varepsilon_3$ parameters of the investigated bianisotropic MM slab with length $L = u_z = 2.54$ mm using the proposed RPI method and RPD method [34] ($L_{01} = L_{02} = 0$) after de-embedding process

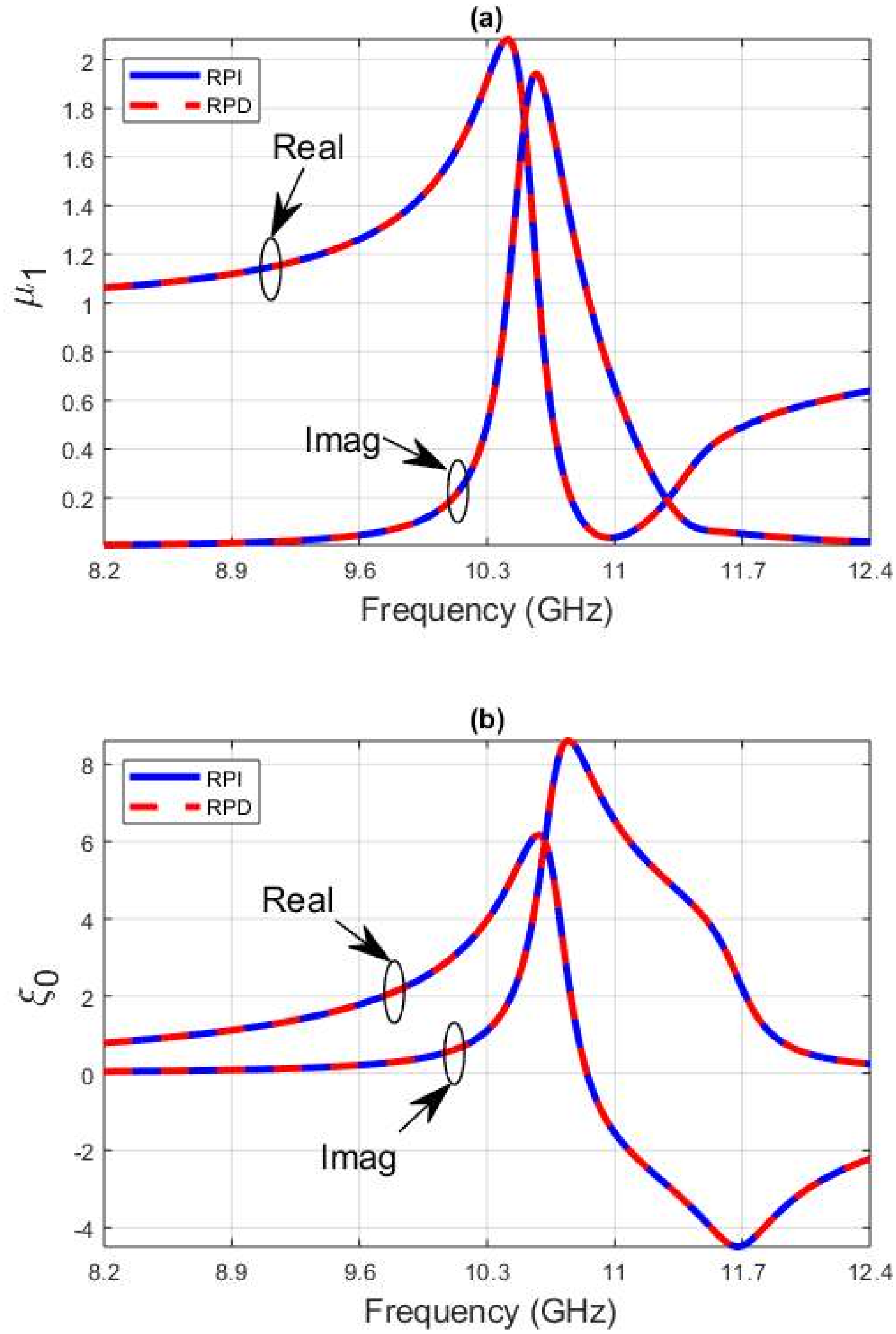


**Figure 3.7** Extracted $\mu_1$ and $\xi_0$ parameters of the investigated bianisotropic MM slab with length $L = u_z = 2.54$ mm using the proposed RPI method and RPD method [34] ($L_{01} = L_{02} = 0$) after de-embedding process

It is noted here, the extracted effective constitutive parameters of the analyzed bianisotropic MM slab obtained by the proposed RPI method of this study are in a good agreement with those obtained by the RPD method proposed in [34]. It would be better to mention that, although the calculated length parameter $L_{01}$ is negative, it is very small and it does not have much influence on extracted constitutive parameters. The results provided in Figures 3.6 and 3.7 demonstrate the accuracy and validation of the proposed RPI method.

In the second type of simulations, the bianisotropic MM sample is simulated by inserting spaces (filled with air) between calibration and measurement planes by non-zero $L_{01}$ and $L_{02}$ values. Thus, the effect of the erroneous distance parameters will be investigated. In accordance with this purpose, the constitutive parameters of the identical bianisotropic MM sample having length $L = u_z = 2.54$ mm are retrieved by using S-parameters obtained by simulation with small length parameters $L_{01} = 0.9$ mm and $L_{02} = 1.1$ mm. In extraction process, firstly $\chi$, $|\Gamma_1|$ and $|\Gamma_2|$ parameters are obtained by the proposed RPI method. The same results are obtained as with the other case (in which $L_{01} = L_{02} = 0$) since the method is reference-plane independent. The results are given in Figure 3.8 and it can be compared with Figure 3.5

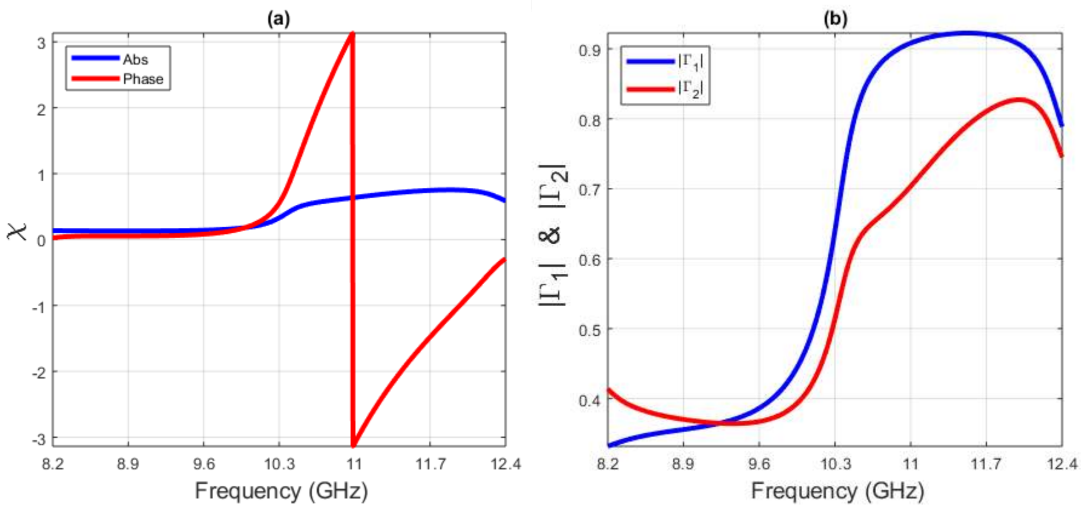


**Figure 3.8** $\chi$, $|\Gamma_1|$ and $|\Gamma_2|$ dependencies of the bianisotropic MM slab with length $L$ = 10.16 mm by the proposed RPI method using S-parameters ($L_{01} = 0.9$ mm, $L_{02} = 1.1$ mm)

Next, the same frequency range (8.8 GHz – 9.7 GHz) and frequency step size ( $\Delta f = 100$ MHz) is selected to determine $e^{i\theta_1}$ and $e^{i\theta_2}$ since having the same dependency pattern as in the previous case, over the X-band. Applying the frequency varying technique, the distance parameters between calibration and measurement planes are calculated as $L_{01}$ = 0.899 mm, $L_{02}$ = 1.101 mm, which are very close to the pre-assigned values in simulation. The same extraction procedure is applied for retrieval of electromagnetic parameters of bianisotropic MM slab with length $L = u_z$ = 2.54 mm. The results are provided in Figures 3.9 and 3.10. Also, the same parameters that extracted with reference-plane dependent method [34] are also provided in the figures to compare the effects of calibration-measurement plane positioning.

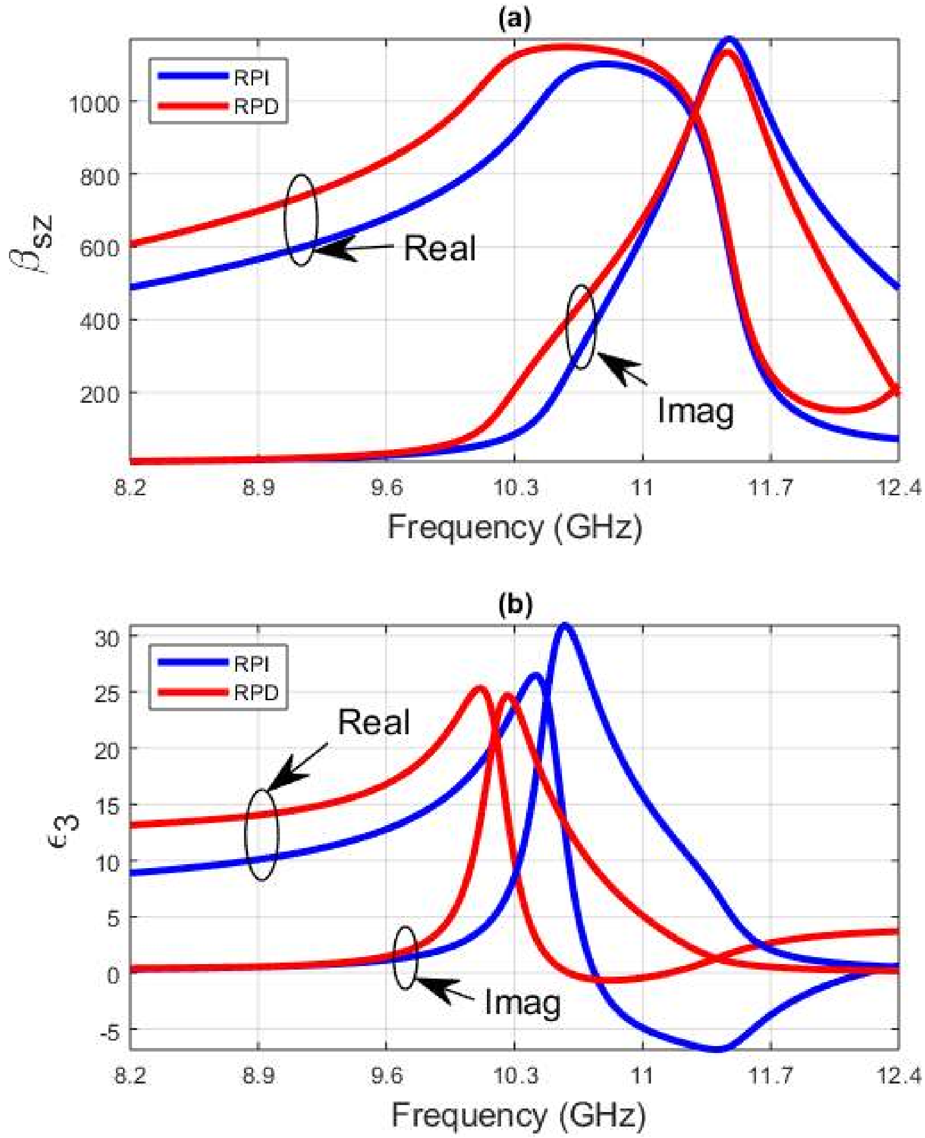


**Figure 3.9** Extracted $\beta_{sz}$ and $\varepsilon_3$ parameters of the investigated bianisotropic MM slab with length $L = u_z$ = 2.54 mm using proposed RPI method and RPD method [34] ($L_{01}$ = 0.9 mm $L_{02}$ = 1.1 mm) after de-embedding process

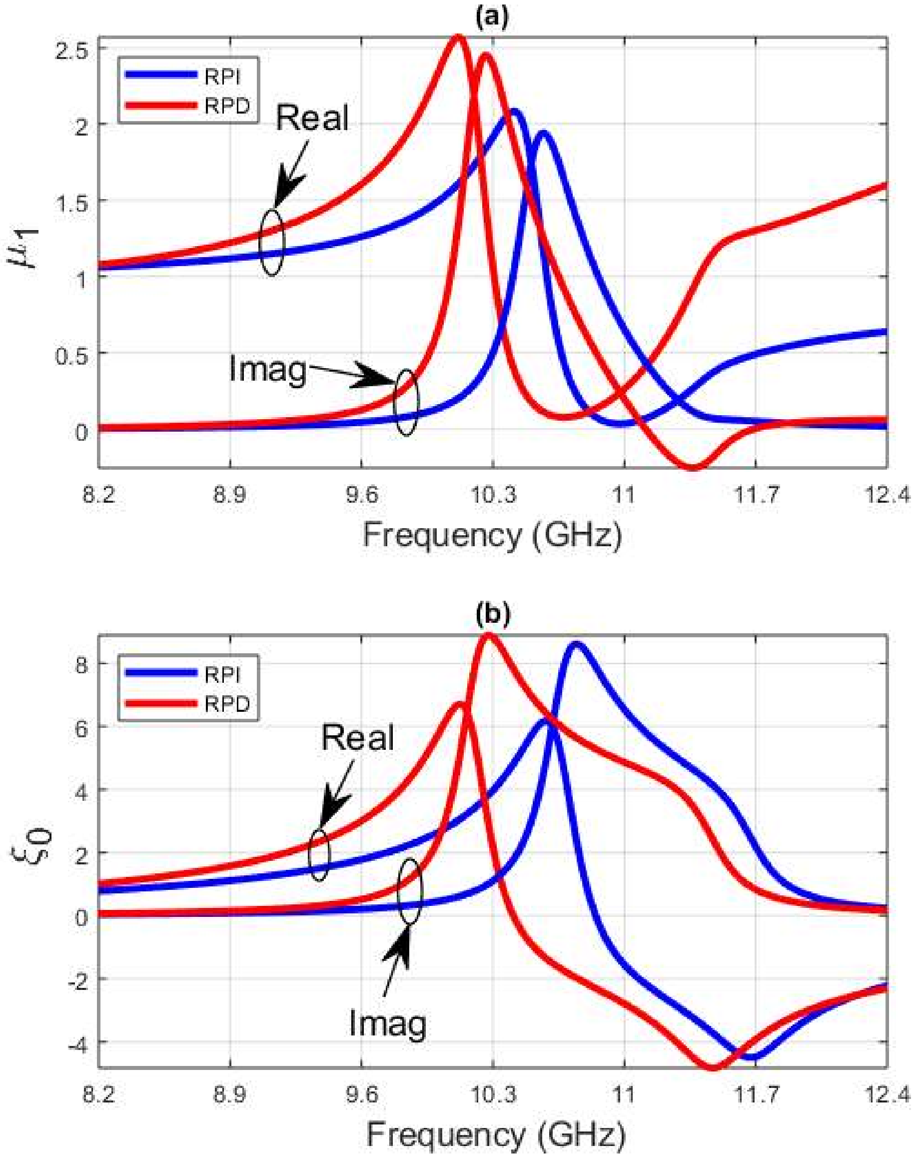


**Figure 3.10** Extracted $\mu_1$ and $\xi_0$ parameters of the investigated bianisotropic MM slab with length $L = u_z = 2.54$ mm using the proposed RPI method and RPD method [34] ($L_{01} = 0.9$ mm $L_{02} = 1.1$ mm) after de-embedding process

When the results for the proposed RPI and the other reference-plane dependent methods are compared, it is noted that, the retrieved constitutive parameters that are shown in Figures 3.9 and 3.10, extracted by the proposed RPI method are very close to those shown in Figures 3.6 and 3.7. Because, the calculated $L_{01}$ and $L_{02}$ values by the proposed method are almost same with the pre-assigned values. This situation points out that, the reference-plane independent feature of the proposed method. It is also noted that, the retrieved constitutive parameters diverge largely from the correct values, which are extracted via reference-plane dependent (RPD) method [34] (when $L_{01} = L_{02} = 0$) even for small changes in $L_{01} = L_{02}$ values (about 1 mm in this case).

## 3.3 Validation of the Proposed Method via Measurements

### 3.3.1 Experimental Setup

In order to further validate the proposed RPI method after performing the numerical simulations, microwave measurement experiments are performed. To generate electromagnetic wave signals propagating through the prepared MM slab and measure its S-parameters, a portable vector network analyzer (VNA) of brand Keysight Instruments (model N9928A) was used. It has an operating frequency range of 30 kHz to 26.5 GHz with a 90 dB of dynamic range (from DC to 18 GHz) and directivity over 32 dB. A picture of the utilized measurement apparatus is given in Figure 3.11.

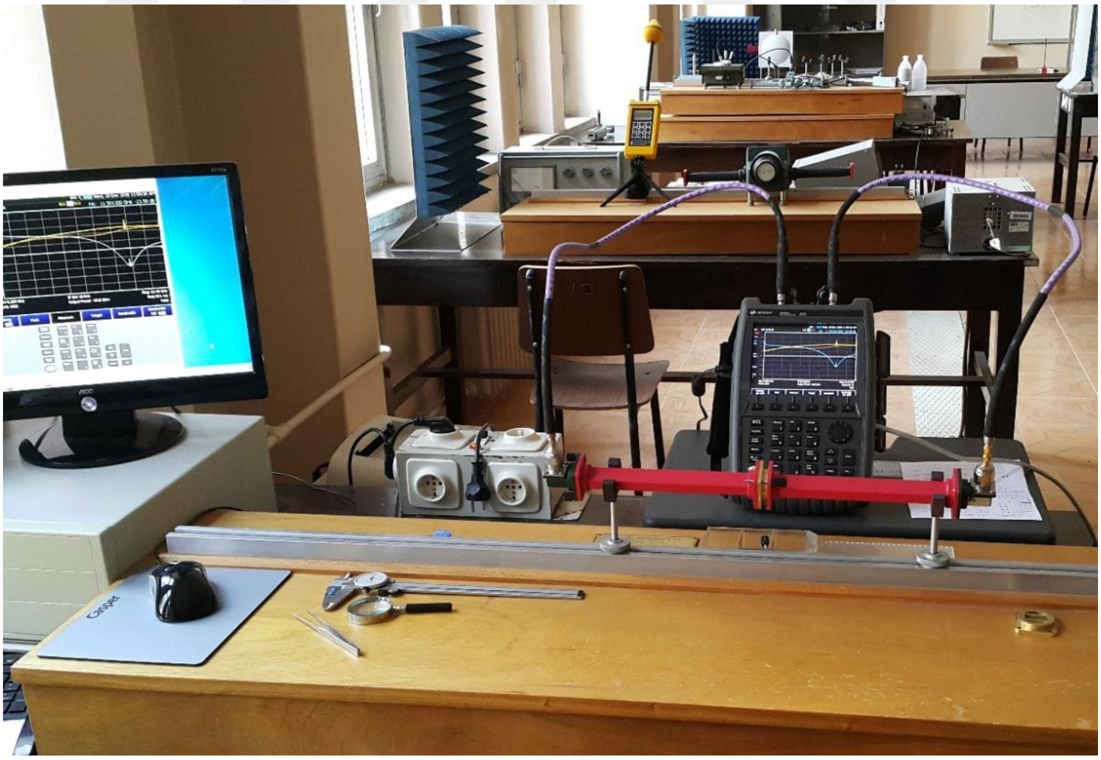

**Figure 3.11** The Experimental apparatus which is used for the validation of the proposed RPI method

The measurements are performed in X-band waveguide and they are properly connected to the VNA. Before starting the measurements, the experimental setup is calibrated by through-reflect-line (TRL) calibration technique. For the TRL method, a 9.4 mm waveguide straight for the line standard (produces at most 70º shift from 90º) and a highly reflective short for the reflect standard are used. After the calibration, its reliability is controlled by analyzing magnitudes of $S_{11}$, $S_{22}$ and $S_{21}$ parameters. The calibration results are $|S_{11}| \cong |S_{22}| < -40$ dB and $|S_{21}| > -0.03$ dB over the entire X-band and demonstrated the accuracy of the TRL calibration method.

### 3.3.2 MM Sample Preparation

The design of MM structure consisting of small unit cells (which is shown in Figure 3.1) was reported in Chapter 3.1. The identical metallic SRR patterns are fabricated on plain FR4 substrates by printed circuit board technique (PCB) and are shown in Figure 3.12. Later, the plain PCBs with each having four printed SRR patterns are divided into square cells (10.16 mm by 10.16 mm) as shown in Figure 3.13 (b). Then, a symmetric sandwiched MM cell is obtained by covering another plain and clean (no pattern) FR4 substrate (shown in Figure 3.13 (a)) with the same size and thickness ($l_s$ = 1.5 mm). Finally, seven pieces of identical MM sandwiches are tightly combined together. However, very small gaps remained to entirely fill the X-band waveguide cross-section. In order to alleviate effects of gap on the extracted constitutive parameters, the remained gaps on both side of the sample are filled with thin (approximately 0.77 mm) and clean FR4 substrates. After the preparation, the sample is inserted into an X-band waveguide section. A photograph of the prepared bianisotropic MM slab with length $L$ = 10.16 mm, in a waveguide section is shown in Figure 3.14.

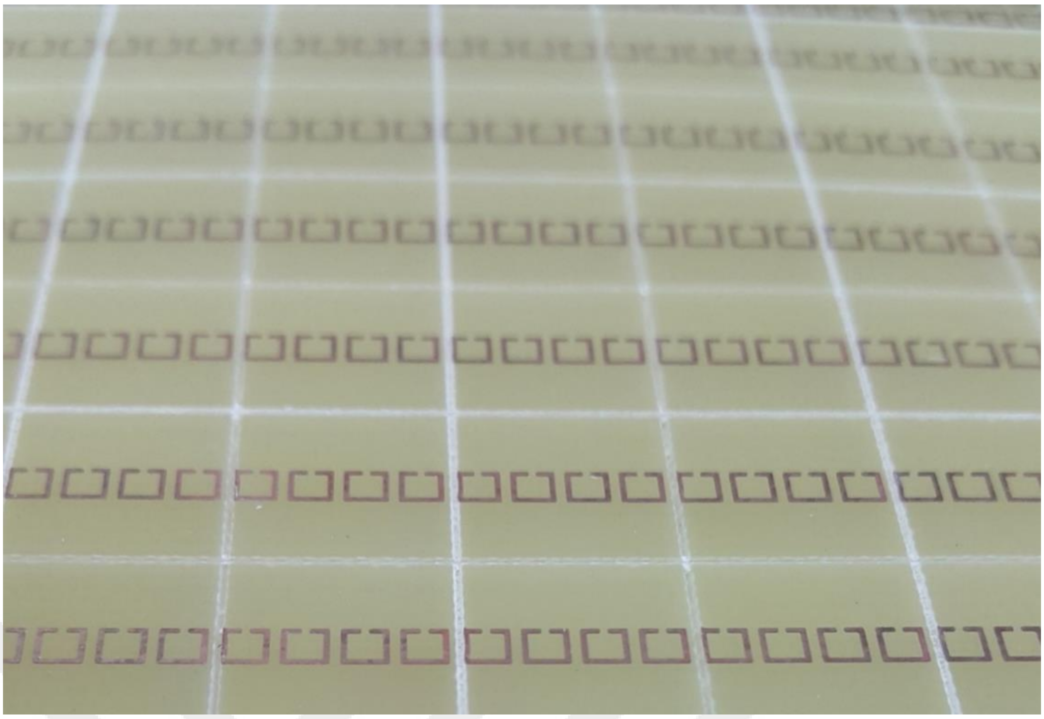

**Figure 3.12** A Printed circuit board (FR4) with divided square shaped cells and metallic SRR patterns printed

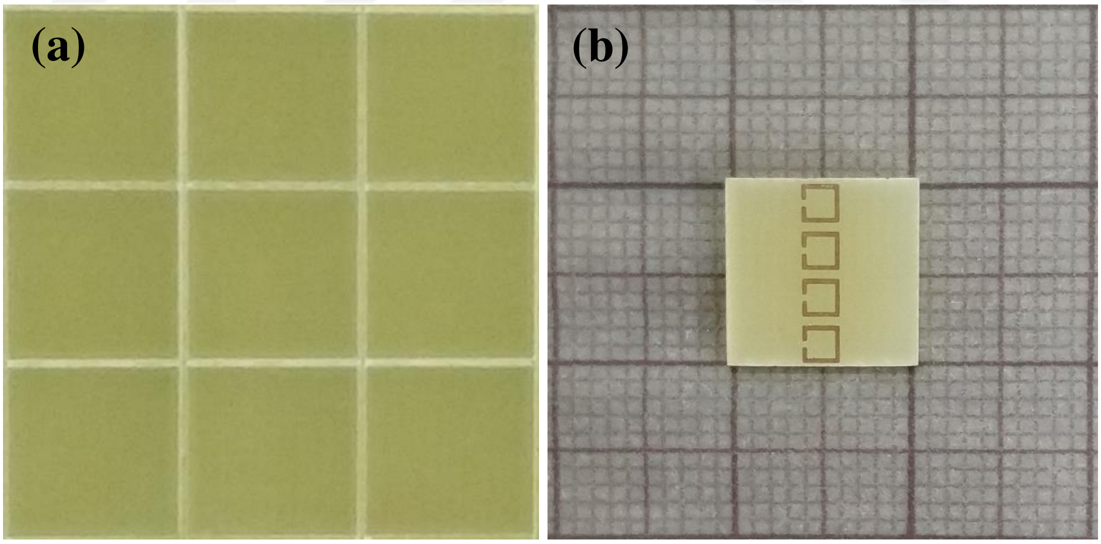


**Figure 3.13** Prepared square (10.16 mm by 10.16 mm) shaped cells ***a)*** *square FR4 substrates with no printed metallic pattern* ***b)*** *a square FR4 substrate with 4 metallic SRR patterns printed on it*

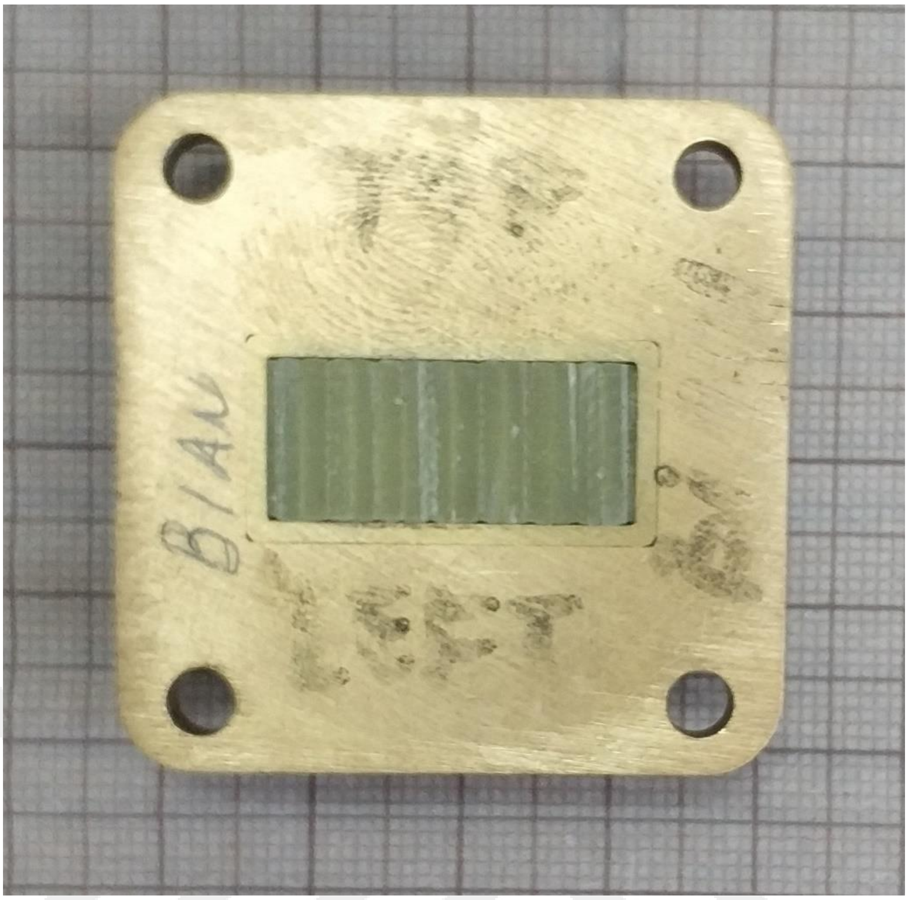

**Figure 3.14** The prepared bianisotropic MM slab with length $L$ = 10.16 mm in a waveguide section includes seven pieces of square sandwiched MM cells

### 3.3.3 Measurements and Discussion

After performing calibration, the prepared slab of MM with length $L$ = 10.16 mm is randomly inserted into an empty waveguide with length 30.21 mm. For the purpose of evaluating the precision of the proposed RPI method, the distances between calibration planes (long waveguide planes) and measurement planes (surface of MM slab) $L_{01} \cong 9.4$ mm and $L_{02} \cong 10.65$ mm are measured by high precision calipers. Then, the S-parameters of the prepared sample are measured by the VNA instrument. The comparison of the measured and simulated (first type, when $L_{01} = L_{02} = 0$) S-parameter magnitudes is shown in Figure 3.15. As it seen, the magnitudes of the measured and simulated reflection S-parameters ($|S_{11}|$ and $|S_{22}|$) have unlike patterns over the whole band which indicates the bianisotropic property of the produced and measured MM slab [29, 34].

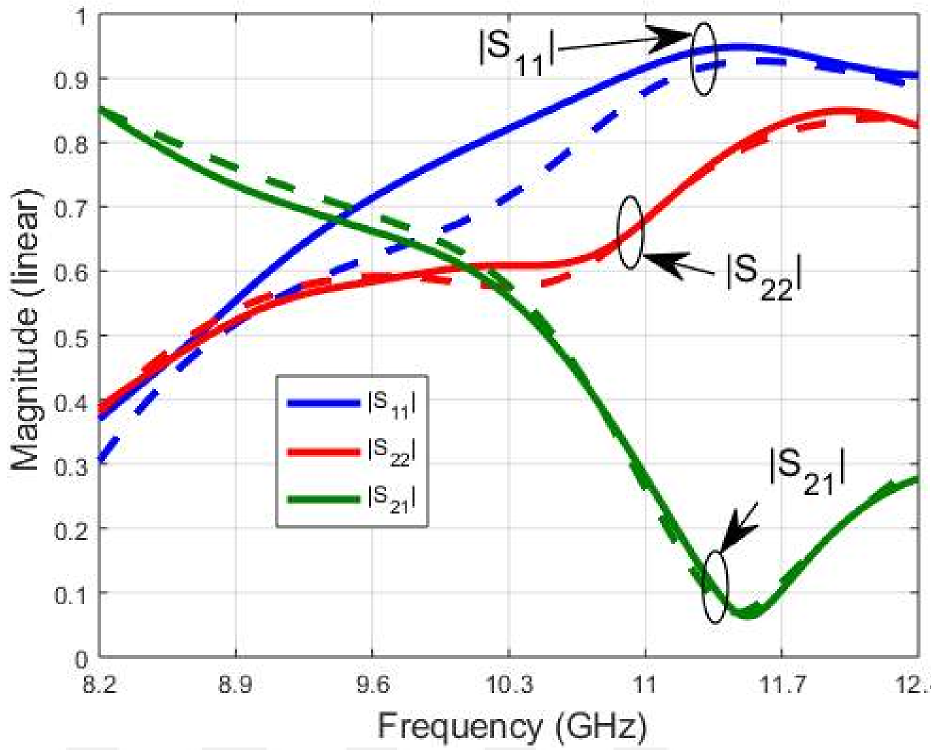


**Figure 3.15** The magnitudes of the measured (continuous lines) and the simulated (dashed lines) S-parameters of the bianisotropic MM slab

The proposed RPI method is implemented without using the distance information $L_{01}$ and $L_{02}$. Firstly, dependency of $\chi$, $|\Gamma_1|$ and $|\Gamma_2|$ parameters over the frequency are extracted using S-parameters and illustrated in Figure 3.16. In the same figure, the dependencies obtained by simulated S-parameters are also shown to make comparison and as it seen measured and simulated values of the parameters are in a good agreement over the entire frequency band.

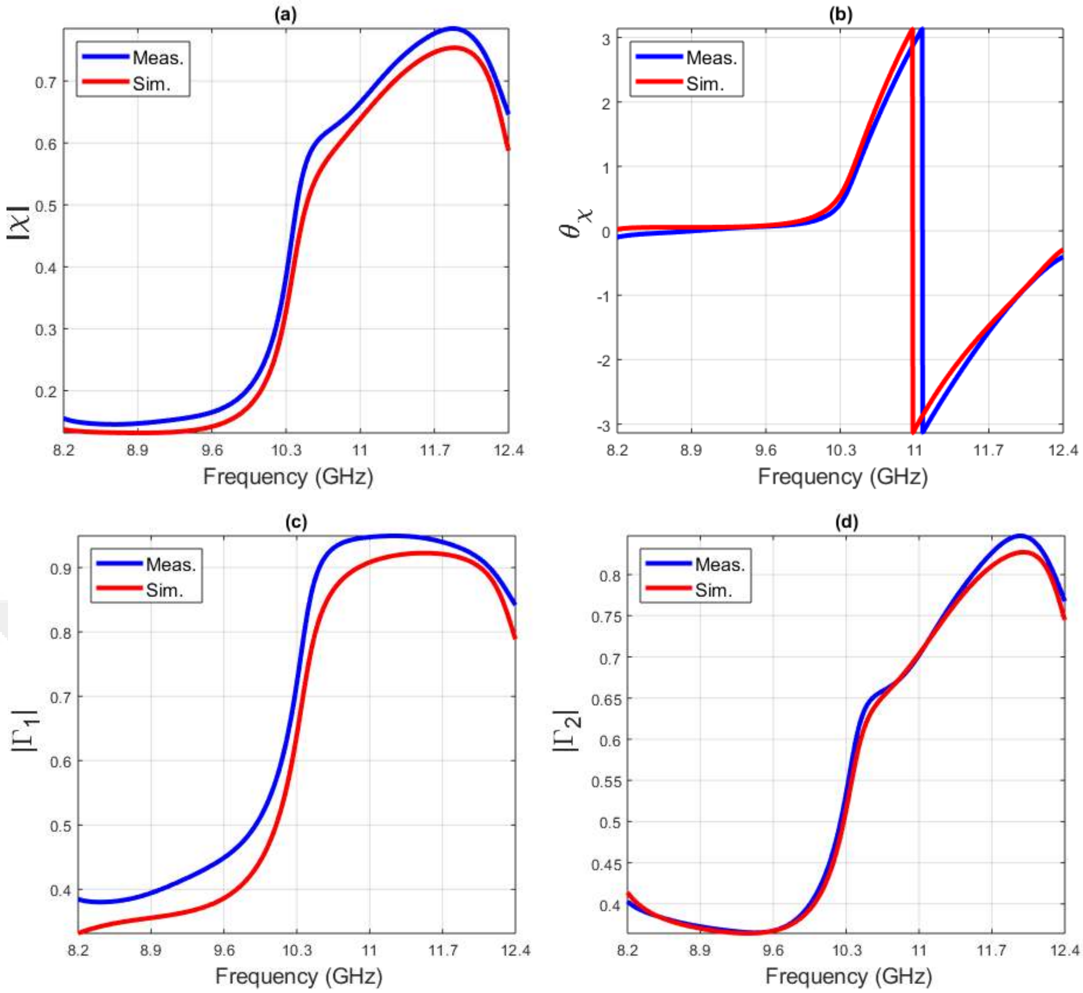


**Figure 3.16** Frequency dependencies of extracted parameters $|\chi|, \theta_\chi$ ,$|\Gamma_1|$ and $|\Gamma_2|$ of the measured and the simulated bianisotropic MM slab with length $L$ = 10.16 mm by the proposed RPI method

Secondly, a frequency region in which the above-determined parameters are constant is should be selected. As seen in Figure 3.16, the frequency range between $f$ = 8.7 GHz and $f$ = 9.7 GHz is a good option to implement the frequency varying technique to measured S-parameters. Distance values $L_{01} \cong 9.357$ mm and $L_{02} \cong 10.693$ mm are calculated with the implementation of the frequency varying technique for $f$ = 8.8 GHz and $\Delta f = 10$ MHz. Then, the calculated distance parameters are used in the extraction of the constitutive parameters of the measured MM slab via S-parameters. The effect of the additional FR4 material in wave propagation direction is eliminated by implementing de-embedding technique where the details are present in Chapter 3.2. The overall results are illustrated in Figures 3.17 – 3.19.

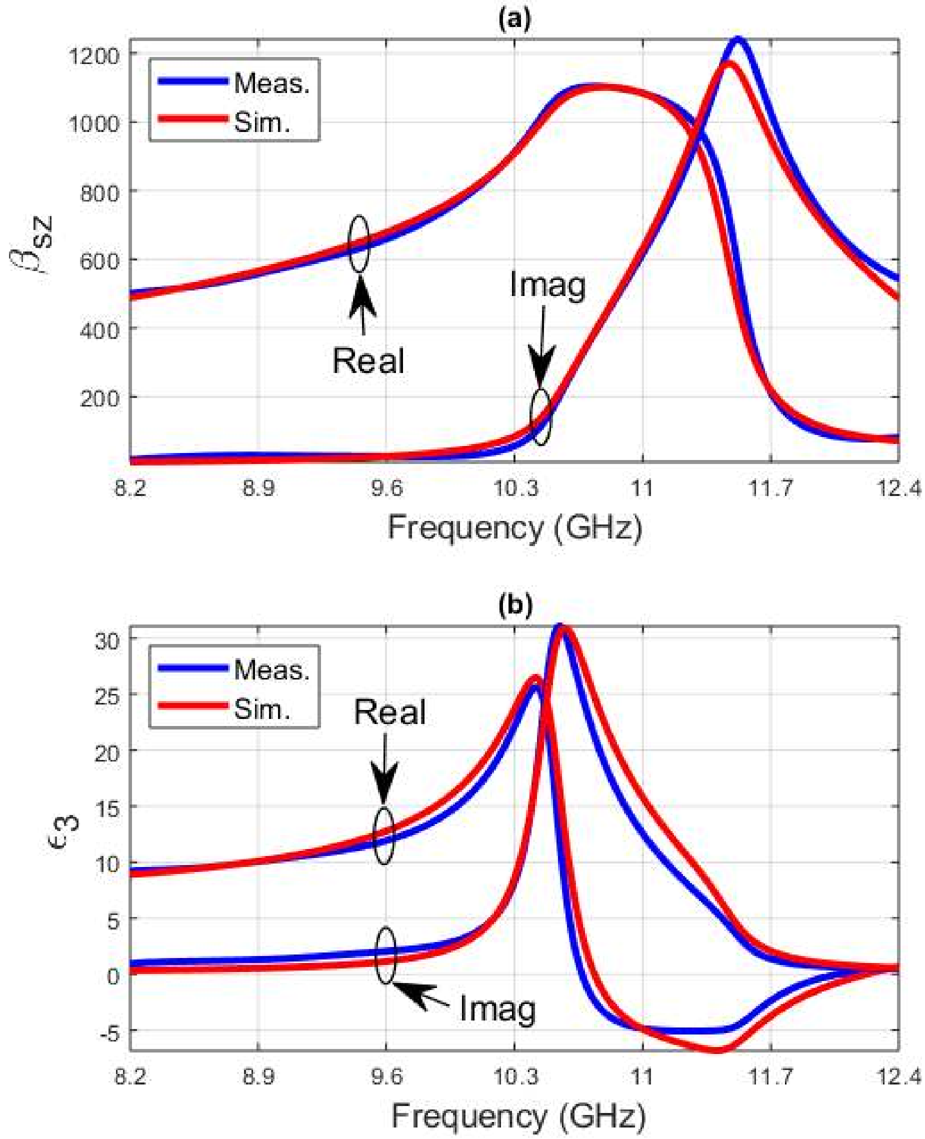


**Figure 3.17** Extracted $\beta_{sz}$ in (a) and $\varepsilon_3$ in (b) of the MM slab with length $L = u_z = 2.54$ mm from the measured and simulated S-parameters by implementation of the RPI method

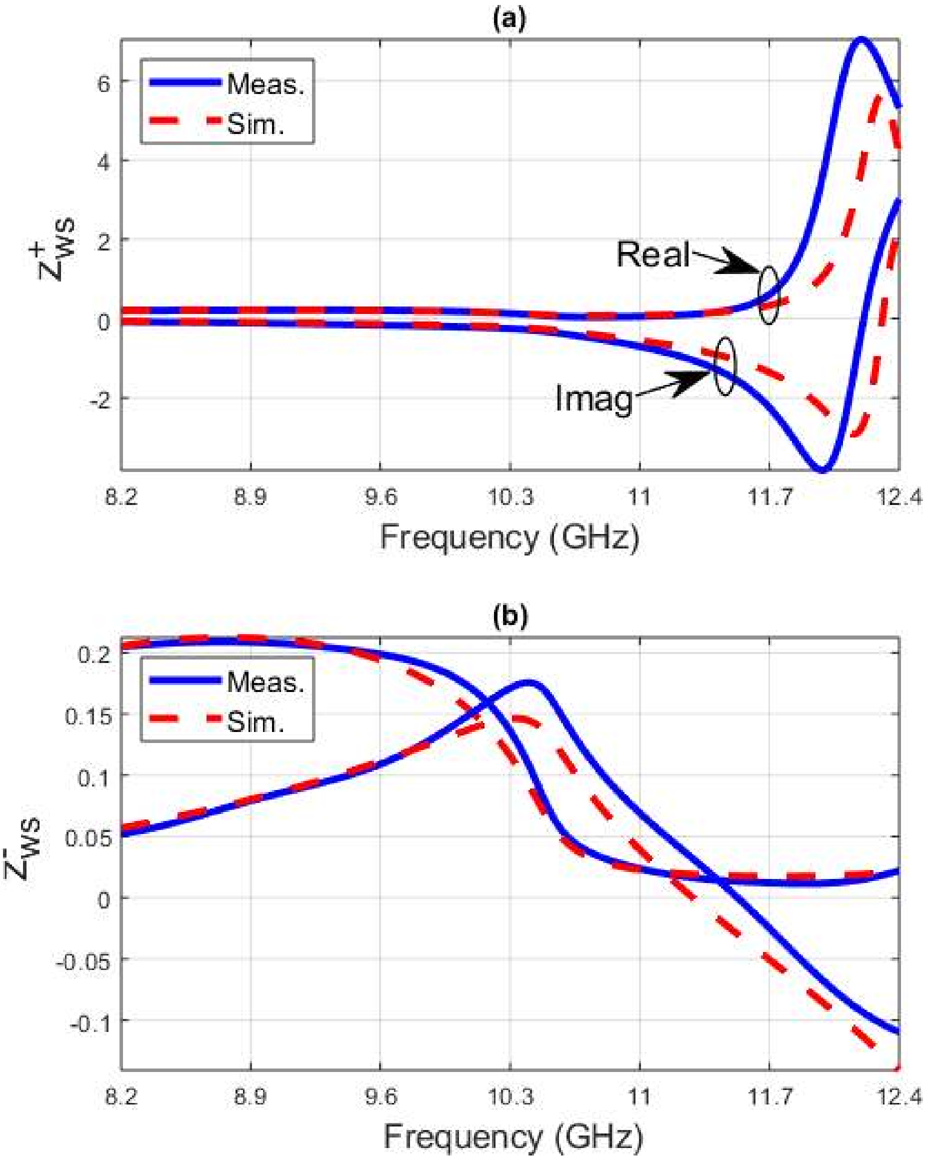


**Figure 3.18** Extracted $z^{+}_{ws}$ in (a) and $z^{-}_{ws}$ in (b) of the MM slab with length $L = u_z = 2.54$ mm from the measured and simulated S-parameters by implementation of the RPI method

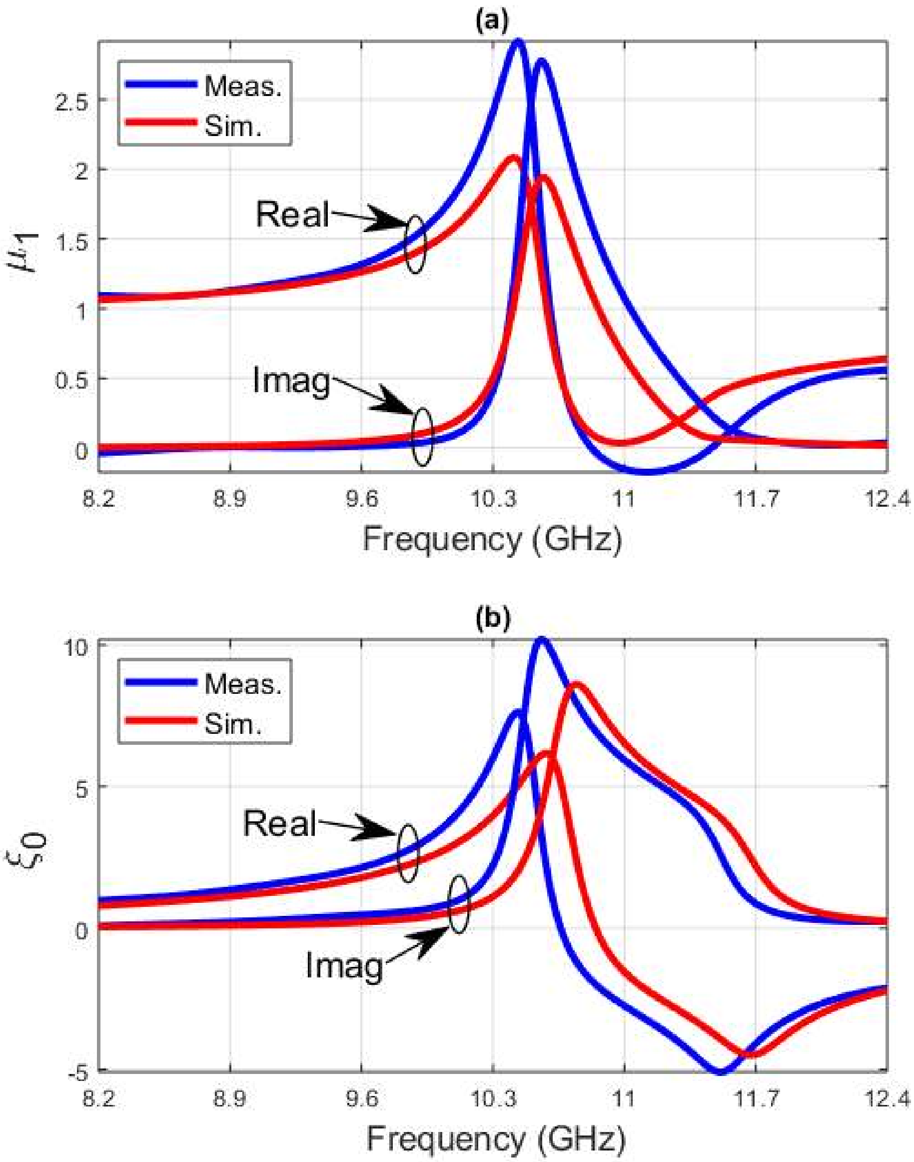


**Figure 3.19** Extracted $\mu_1$ in (a) and $\xi_0$ in (b) of the MM slab with length $L = u_z = 2.54$ mm from the measured and simulated S-parameters by implementation of the RPI method

When the obtained results are analyzed, the following important points are noted. Firstly, the retrieved constitutive parameters $\beta_{sz}$, $\varepsilon_3$, $z_{ws}^{+}$, $z_{ws}^{-}$, $\mu_1$ and $\xi_0$ obtained by the proposed RPI method via measurements are in a good agreement with those retrieved by the simulations for $L_{01} = L_{02} = 0$. It is validated that the retrieval of constitutive parameters of a bianisotropic MM slab without knowledge of reference plane information. However, small deviations in amplitudes and frequencies may observed between retrieved experimental and simulation data, since it is very difficult to fabricate perfect and exact samples as in simulations. These deviations may arise from the fabrication tolerances such as geometrical and constructional imperfections and very tiny air gaps between FR4 layers. Fortunately, the obtained results are very satisfactory for the fabricated MM samples with PCB technique. Secondly, the retrieved constitutive parameters fulfil passivity, causality and power-dissipation, the locality conditions [68]. For instance, all of the $\mathrm{Im}\{n_s\}(\beta_{sz}/k_0)$, $\mathrm{Re}\{z_{ws}^{+}\}$ and $\mathrm{Re}\{z_{ws}^{-}\}$ parameters are positive, means that the passivity condition is satisfied. Also, $\mathrm{Re}\{\varepsilon_3\}$ and $\mathrm{Re}\{\mu_1\}$ increase with the frequency in 8.2 10.3 GHz band over which there is negligible dissipative losses. Lastly, the power dissipation condition is satisfied for $\mathrm{Re}\{z_{ws}^{+}\}>0$ and $\mathrm{Re}\{z_{ws}^{-}\}>0$ as a result of the existing medium loss in the MM slab due to loss of substrate and conductor [34].

It is noted that the RPI method is dependent to the length *L* of the analyzed MM slab. Thus, accurate length of the sample is necessary to implement the RPI method for the constitutive parameter retrieval. The length of the MM slab may not correspond to its coarse physical dimension due to non-negligible boundary effects around the edges of the slab [26,69]. Because, the length of lossy dielectric FR4 material ($L$ = 10.16 mm) which involves the MM unit cell in *z*-axis, is much bigger than the length of MM unit cell ($u_z$ = 2.54 mm) and it is thought that, due to this reason the higher order modes around SRRs decrease towards the ending boundary of the FR4 material.

In order to specify the effective length of a MM slab with non-negligible boundary effects, the method [70] which minimizes the differences of wave impedances of identical MM slabs having different lengths may be implemented and it will be considered as a future study.

Now, for demonstrating the effect of variation of the MM slab length the constitutive parameters, $\mu_1$ and $\xi_0$ of the sample and identical sample having small deviation (5% offset) in its length ($L$ = 1.05×2.54 mm = 2.667 mm) are retrieved. The results are illustrated in Figure 3.20. It is noted that, the retrieved parameters $\mu_1$ and $\xi_0$ of the MM slabs having different lengths, differ especially in 9.5 – 10.7 GHz region (higher order modes) where sharp changes occur in values of the parameters.

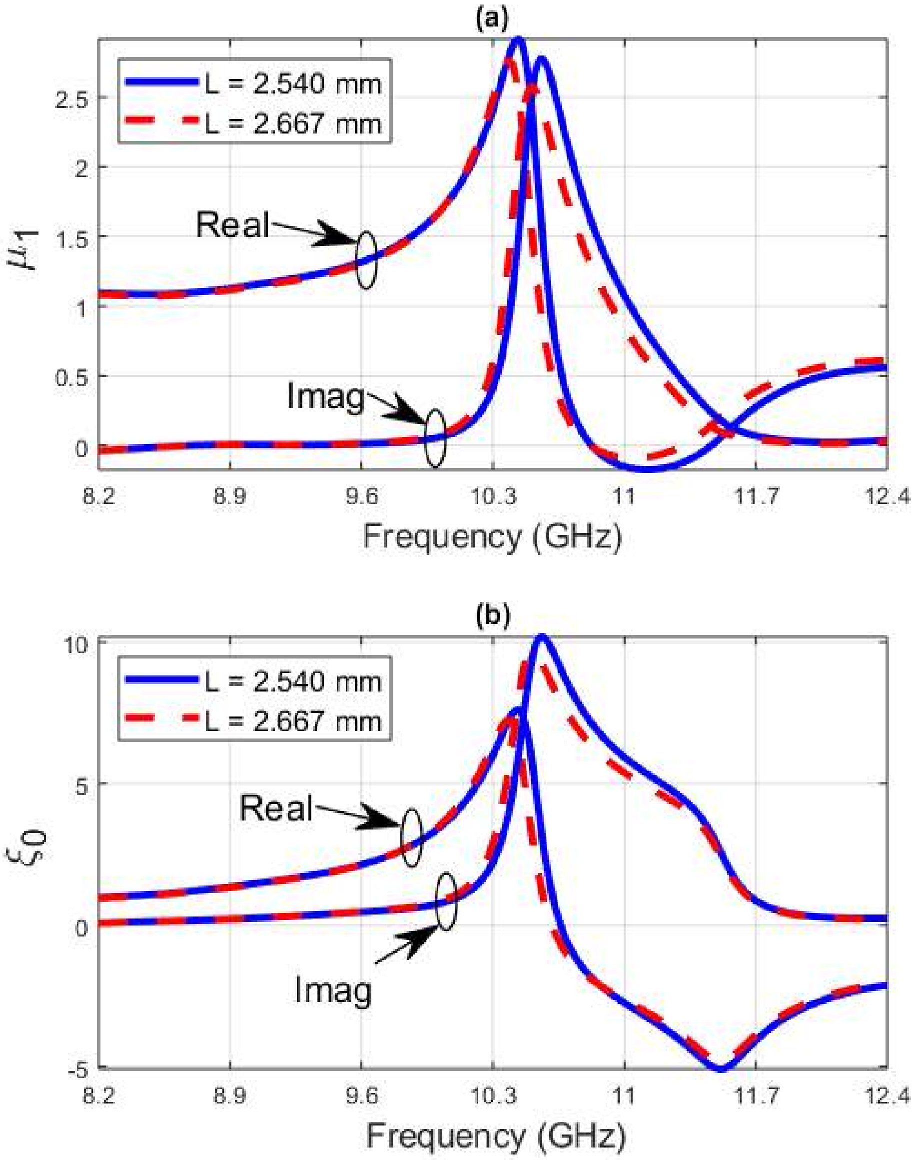


**Figure 3.20** Extracted $\mu_1$ in (a) and $\xi_0$ in (b) of the MM slab with length $L = u_z = 2.54$ mm with/without +5% offset from the measured and simulated S-parameters by implementation of the RPI method

# CHAPTER 4

# CONCLUSION

In this study, retrieval of effective constitutive parameters of biaxial bianisotropic MM slabs by using reference-plane-invariant (RPI) method is investigated. Rectangular waveguides are used to extract scattering (S-) parameters in X-band frequency range. For that purpose, the frequency varying method is proposed and applied to extract separate reflection coefficients of bianisotropic MM slabs. A MM slab having bianisotropic property that consisting of single ring SRR unit cells is designed and produced for the simulations and measurement experiments. The designed MM slab is primarily simulated and then the real experiments are conducted by fabricating the designed MM slab. A vector network analyzer is used to retrieve S-parameters of the measured sample. In order to validate the proposed retrieval method, the desired effective constitutive parameters of the simulated/measured MM slab are obtained from S-parameters and then these parameters are compared with the parameters obtained by another method which is dependent on reference plane positions. Also noting that, this reference-plane dependent method is severely affected by any inaccurate reference plane information.

It is demonstrated in this study that the effective constitutive parameters of the biaxial bianisotropic MM sample is accurately extracted by the proposed RPI method and without knowing reference plane location information. The results are obtained by numerical simulations and measurement experiments are reported.

It should be denoted that, in this study a MM slab that consists of multiple one-cell substructures, along the wave propagation direction is fabricated and used. Although accurately evaluating the lengths of the analyzed MM slab, the retrieved constitutive parameters of more than one-cell along wave propagation direction may not correspond to constitutive parameters of one-cell MM slab, by using RPI method. Because, along the wave propagation direction, a coupling effect between neighboring SRR structures is formed and this affect the overall characteristics of the MM slab [19]. As a future work, further studies may be performed to analyze and reveal the effects of this coupling phenomenon.

## REFERENCES


[1] Veselago, V. G. (1967). Electrodynamics of Substances with Simultaneously Negative Electrical and Magnetic Permeabilities, *Usp. Fiz. Nauk*. **92**, 517.

[2] Chen, T., Li, S., Sun, H. (2012). Metamaterials Application in Sensing, *Sensors*. **12(3)**, 2742-2765.

[3] Yoo, Y. J., Ju, S., Park, S. Y., Kim, Y. J., Bong, J., Lim, T., ..., Lee, Y. (2015). Metamaterial Absorber for Electromagnetic Waves in Periodic Water Droplets, *Scientific Reports.* **5**, 14018.

[4] Schurig, D., Mock, J. J., Justice, B. J., Cummer, S. A., Pendry, J. B., Starr, A. F., Smith, D. R. (2006). Metamaterial Electromagnetic Cloak at Microwave Frequencies, *Science.* **314(5801)**, 977-980.

[5] Zhang, J., Luo, Y., Chen, H., Wu, B. I. (2008). Manipulating the Directivity of Antennas with Metamaterial, *Optics Express*. **16(15)**, 10962-10967.

[6] Pendry, J. B., Holden, A. J., Stewart, W. J., Youngs, I. (1996). Extremely Low Frequency Plasmons in Metallic Mesostructures, *Physical Review Letters*. **76(25)**, 4773.

[7] Pendry, J. B., Holden, A. J., Robbins, D. J., Stewart, W. J. (1999). Magnetism from Conductors and Enhanced Nonlinear Phenomena, *IEEE Transactions on Microwave Theory and Techniques*. **47(11)**, 2075-2084.

[8] Smith, D. R., Padilla, W. J., Vier, D. C., Nemat-Nasser, S. C., Schultz, S. (2000). Composite Medium with Simultaneously Negative Permeability and Permittivity, *Physical Review Letters*. **84(18)**, 4184.

[9] Tal, Eran (2017). Measurement in Science, *The Stanford Encyclopedia of Philosophy.*

[10] Queffelec, P., Laur, V., Chevalier, A., Le Floch, J. M., Passerieux, D., Cros, D., ..., Houzet, G. (2014). Intercomparison of Permittivity Measurement Techniques for Ferroelectric Thin Layers, *Journal of Applied Physics.* **115(2)**, 024103.

[11] Pendry, J. B., Holden, A. J., Robbins, D. J., Stewart, W. J. (1998). Low Frequency Plasmons in Thin-Wire Structures, *Journal of Physics: Condensed Matter.* **10(22)**, 4785.

[12] Marqués, R., Medina, F., Rafii-El-Idrissi, R. (2002). Role of Bianisotropy in Negative Permeability and Left-Handed Metamaterials, *Physical Review B*. **65(14)**, 144440.

[13] Lubkowski, G., Schuhmann, R., Weiland, T. (2007). Extraction of Effective Metamaterial Parameters by Parameter Fitting of Dispersive Models, *Microwave and Optical Technology Letters*. **49(2)**, 285-288.

[14] Alu, A. (2011). First-Principles Homogenization Theory for Periodic Metamaterials, *Physical Review B*. **84(7)**, 075153.

[15] Arslanagić, S., Hansen, T. V., Mortensen, N. A., Gregersen, A. H., Sigmund, O., Ziolkowski, R. W., Breinbjerg, O. (2013). A Review of the Scattering-Parameter Extraction Method with Clarification of Ambiguity Issues in Relation to Metamaterial Homogenization, *IEEE Antennas and Propagation Magazine*. **55(2)**, 91-106.

[16] Chen, L., Ong, C. K., Tan, B. T. G. (1999). Cavity Perturbation Technique for the Measurement of Permittivity Tensor of Uniaxially Anisotropic Dielectrics, *IEEE Transactions on Instrumentation and Measurement*. **48(6)**, 1023-1030.

[17] Belhadj-Tahar, N. E., Fourrier-Lamer, A. (1991). Broad-Band Simultaneous Measurement of the Complex Permittivity Tensor for Uniaxial Materials using a Coaxial Discontinuity, *IEEE Transactions on Microwave Theory and Techniques*. **39(10)**, 1718-1724.

[18] Queffelec, P., Laur, V., Chevalier, A., Le Floch, J. M., Passerieux, D., Cros, D., ..., Houzet, G. (2014). Intercomparison of Permittivity Measurement Techniques for Ferroelectric Thin Layers, *Journal of Applied Physics*. **115(2)**, 024103.

[19] Shi, Y., Li, Z. Y., Li, K., Li, L., Liang, C. H. (2017). A Retrieval Method of Effective Electromagnetic Parameters for Inhomogeneous Metamaterials, *IEEE Transactions on Microwave Theory and Techniques*. **65(4)**, 1160-1178.

[20] Smith, D. R., Vier, D. C., Koschny, T., Soukoulis, C. M. (2005). Electromagnetic Parameter Retrieval from Inhomogeneous Metamaterials, *Physical Review E*. **71(3)**, 036617.

[21] Hasar, U. C., Barroso, J. J., Buldu, G., Bute, M., Kaya, Y., Karacali, T., Ertugrul, M. (2014). Reference-Plane-Invariant Effective Thickness and Electromagnetic Property Determination of Isotropic Metamaterials Involving Boundary Effects, *IEEE Journal of Selected Topics in Quantum Electronics*. **21(4)**, 301-311.

[22] Jiang, Z. H., Bossard, J. A., Wang, X., Werner, D. H. (2011). Synthesizing Metamaterials with Angularly Independent Effective Medium Properties Based on an Anisotropic Parameter Retrieval Technique Coupled with a Genetic Algorithm, *Journal of Applied Physics*. **109(1)**, 013515.

[23] Driscoll, T., Basov, D. N., Padilla, W. J., Mock, J. J., Smith, D. R. (2007). Electromagnetic Characterization of Planar Metamaterials by Oblique Angle Spectroscopic Measurements, *Physical Review B*. **75(11)**, 115114.

[24] Menzel, C., Rockstuhl, C., Paul, T., Lederer, F., Pertsch, T. (2008). Retrieving Effective Parameters for Metamaterials at Oblique Incidence, *Physical Review B*. **77(19)**, 195328.

[25] Hasar, U. C., Barroso, J. J., Sabah, C., Kaya, Y., Ertugrul, M. (2013). Stepwise Technique for Accurate and Unique Retrieval of Electromagnetic Properties of Bianisotropic Metamaterials, *JOSA B*. **30(4)**, 1058-1068.

[26] Hasar, U. C., Barroso, J. J., Bute, M., Muratoglu, A., Ertugrul, M. (2016). Boundary Effects on the Determination of Electromagnetic Properties of Bianisotropic Metamaterials from Scattering Parameters, *IEEE Transactions on Antennas and Propagation*. **64(8)**, 3459-3469.

[27] Cohen, D., Shavit, R. (2015). Bi-anisotropic Metamaterials Effective Constitutive Parameters Extraction using Oblique Incidence S-parameters Method, *IEEE Transactions on Antennas and Propagation.* **63(5)**, 2071-2078.

[28] Chen, X., Wu, B. I., Kong, J. A., Grzegorczyk, T. M. (2005). Retrieval of the Effective Constitutive Parameters of Bianisotropic Metamaterials, *Physical Review E*. **71(4)**, 046610.

[29] Li, Z., Aydin, K., Ozbay, E. (2009). Determination of the Effective Constitutive Parameters of Bianisotropic Metamaterials from Reflection and Transmission Coefficients, *Physical Review E*. ***79*(2)**, 026610.

[30] Hasar, U. C. (2009). A Microwave Method for Noniterative Constitutive Parameters Determination of Thin Low-Loss or Lossy Materials, *IEEE Transactions on Microwave Theory and Techniques*. **57(6)**, 1595-1601.

[31] Hasar, U. C., Westgate, C. R. (2009). A Broadband and Stable Method for Unique Complex Permittivity Determination of Low-Loss Materials, *IEEE Transactions on Microwave Theory and Techniques*. **57(2)**, 471-477.

[32] Trang, F., Rogalla, H., Popović, Z. (2014). Effective Constitutive Parameters of High-Temperature Superconducting Split-Ring Resonator Arrays, *IEEE Transactions on Applied Superconductivity*. **25(1)**, 1-7.

[33] Chen, H., Zhang, J., Bai, Y., Luo, Y., Ran, L., Jiang, Q., Kong, J. A. (2006). Experimental Retrieval of the Effective Parameters of Metamaterials Based on a Waveguide Method, *Optics Express*. **14(26)**, 12944-12949.

[34] Hasar, U. C., Muratoglu, A., Bute, M., Barroso, J. J., Ertugrul, M. (2017). Effective Constitutive Parameters Retrieval Method for Bianisotropic Metamaterials using Waveguide Measurements, *IEEE Transactions on Microwave Theory and Techniques*. **65(5)**, 1488-1497.

[35] Hasar, U. C., Buldu, G., Barroso, J. J. (2017). Waveguide Method for Electromagnetic Parameter Extraction of Weakly Coupled Metamaterials, *IEEE Microwave and Wireless Components Letters*. **27(9)**, 851-853.

[36] Smith, D. R., Schultz, S., Markoš, P., Soukoulis, C. M. (2002). Determination of Effective Permittivity and Permeability of Metamaterials from Reflection and Transmission Coefficients, *Physical Review B*. **65(19)**, 195104.

[37] Hasar, U. C., Barroso, J. J., Karacali, T., Ertugrul, M. (2015). Reference-Plane-Invariant and Thickness and Branch-Index-Independent Retrieval of Effective Parameters of Bi-anisotropic Metamaterials, *AIP Advances*. **5(1)**, 017123.

[38] Hasar, U. C., Kaya, Y., Barroso, J. J., Ertugrul, M. (2015). Determination of Reference-Plane Invariant, Thickness-Independent, and Broadband Constitutive Parameters of Thin Materials, *IEEE Transactions on Microwave Theory and Techniques*. **63(7)**, 2313-2321.

[39] Chalapat, K., Sarvala, K., Li, J., Paraoanu, G. S. (2009). Wideband Reference-Plane Invariant Method for Measuring Electromagnetic Parameters of Materials, *IEEE Transactions on Microwave Theory and Techniques*. **57(9)**, 2257-2267.

[40] Baker-Jarvis, J., Vanzura, E. J., Kissick, W. A. (1990). Improved Technique for Determining Complex Permittivity with the Transmission/Reflection Method, *IEEE Transactions on Microwave Theory and Techniques*. **38(8)**, 1096-1103.

[41] Hasar, U. C., Kaya, Y., Bute, M., Barroso, J. J., Ertugrul, M. (2014). Microwave Method for Reference-Plane-Invariant and Thickness-Independent Permittivity Determination of Liquid Materials, *Review of Scientific Instruments*. **85(1)**, 014705.

[42] Hasar, U. C., Barroso, J. J., Bute, M., Kaya, Y., Kocadagistan, M. E., Ertugrul, M. (2014). Attractive Method for Thickness-Independent Permittivity Measurements of Solid Dielectric Materials, *Sensors and Actuators A: Physical*. **206**, 107-120.

[43] Hasar, U. C., Barroso, J. J., Sabah, C., Ozbek, I. Y., Kaya, Y., Dal, D., Aydin, T. (2012). Retrieval of Effective Electromagnetic Parameters of Isotropic Metamaterials Using Reference-Plane Invariant Expressions, *Progress In Electromagnetics Research.* **132**, 425-441.

[44] Buriak, I. A., Zhurba, V. O., Vorobjov, G. S., Kulizhko, V. R., Kononov, O. K., Rybalko, O. (2016). Metamaterials: Theory, Classification and Application Strategies, *Журнал нано-та електронної фізики*. (8,№ **4** (**2**)), 04088-1.

[45] Awai, I., Matsuda, I., Hotta, M., Sanada, A., Kubo, H. (2006). Microwave Applications of Single Negative Materials, *Journal of the European Ceramic Society*. **26(10-11)**, 1811-1815.

[46] Caloz, C., Itoh, T. (2005). *Electromagnetic metamaterials: transmission line theory and microwave applications*. John Wiley & Sons.

[47] Pendry, J. B., Holden, A. J., Robbins, D. J., Stewart, W. J. (1998). Low Frequency Plasmons in Thin-Wire Structures, *Journal of Physics: Condensed Matter*. **10(22)**, 4785.

[48] Schurig, D., Mock, J. J., Smith, D. R. (2006). Electric-Field-Coupled Resonators for Negative Permittivity Metamaterials, *Applied Physics Letters.* **88(4)**, 041109.

[49] Falcone, F., Lopetegi, T., Laso, M. A. G., Baena, J. D., Bonache, J., Beruete, M., ..., Sorolla, M. (2004). Babinet Principle Applied to the Design of Metasurfaces and Metamaterials, *Physical Review Letters*. **93(19)**, 197401.

[50] Liu, R., Degiron, A., Mock, J. J., Smith, D. R. (2007). Negative Index Material Composed of Electric and Magnetic Resonators, *Applied Physics Letters*. **90(26)**, 263504.

[51] Dhouibi, A., Burokur, S. N., de Lustrac, A., Priou, A. (2012). Comparison of Compact Electric-LC Resonators for Negative Permittivity Metamaterials, *Microwave and Optical Technology Letters*. **54(10)**, 2287-2295.

[52] Hudlicka, M., Machac, J., Nefedov, I. S. (2006). A Triple Wire Medium as an Isotropic Negative Permittivity Metamaterial, *Progress In Electromagnetics Research*. **65**, 233-246.

[53] Ozbay, E., Guven, K., Aydin, K. (2007). Metamaterials with Negative Permeability and Negative Refractive Index: Experiments and Simulations, *Journal of Optics A: Pure and Applied Optics*. ***9(9)***, S301.

[54] Smith, D. R., Pendry, J. B., Wiltshire, M. C. (2004). Metamaterials and Negative Refractive Index, *Science*. **305(5685)**, 788-792.

[55] Ekmekci, E. (2010). Design Fabrication and Characterization of Novel Metamaterials in Microwave and Terahertz Regions: Multi-Band Frequency-Tunable and Miniaturized Structure. *Middle East Technical University*.

[56] Marqués, R., Mesa, F., Martel, J., Medina, F. (2003). Comparative Analysis of Edge and Broadside-Coupled Split Ring Resonators for Metamaterial Design Theory and Experiments, *IEEE Transactions on Antennas and Propagation*. **51(10)**, 2572-2581.

[57] Itoh, T. (2004). Prospects for Metamaterials, *Electronics Letters.* **40(16)**, 972-973.

[58] Mackay, T. G., Lakhtakia, A. (2010). *Electromagnetic Anisotropy and Bianisotropy: A Field Guide*. World Scientific.

[59] Chen, X., Wu, B. I., Kong, J. A., Grzegorczyk, T. M. (2005). Retrieval of the Effective Constitutive Parameters of Bianisotropic Metamaterials, *Physical Review E*. **71(4)**, 046610.

[60] Hasar, U. C., Yildiz, G., Bute, M., Muratoglu, A. (2018). Reference-Plane-Invariant Waveguide Method for Electromagnetic Characterization of Bi-axial Bianisotropic Metamaterials, *Sensors and Actuators A: Physical*. **283**, 141-150.

[61] Damaskos, N. J., Mack, R. B., Maffett, A. L., Parmon, W., Uslenghi, P. L. E. (1984). The Inverse Problem for Biaxial Materials, *IEEE Transactions on Microwave Theory and Techniques*. **32(4)**, 400-405.

[62] Wang, S., Niu, M., Xu, D. (1998). A Frequency-Varying Method for Simultaneous Measurement of Complex Permittivity and Permeability with an Open-Ended Coaxial Probe, *IEEE Transactions on Microwave Theory and Techniques*. **46(12)**, 2145-2147.

[63] Hasar, U. C., Simsek, O., Aydin, A. C. (2010). Application of Varying-Frequency Amplitude-Only Technique for Electrical Characterization of Hardened Cement-Based Materials, *Microwave and Optical Technology Letters*. **52(4)**, 801-805.

[64] Xu, X. L., Quan, B. G., Gu, C. Z., Wang, L. (2006). Bianisotropic Response of Microfabricated Metamaterials in the Terahertz Region, *JOSA B*. **23(6)**, 1174-1180.

[65] Jing, X., Xia, R., Wang, W., Tian, Y., Hong, Z. (2016). Determination of the Effective Constitutive Parameters of Bianisotropic Planar Metamaterials in the Terahertz Region, *JOSA A*. **33(5)**, 954-961.

[66] Kriegler, C. E., Rill, M. S., Linden, S., Wegener, M. (2009). Bianisotropic Photonic Metamaterials, *IEEE Journal of Selected Topics in Quantum Electronics*. **16(2)**, 367-375.

[67] Ghodgaonkar, D. K., Varadan, V. V., Varadan, V. K. (1990). Free-Space Measurement of Complex Permittivity and Complex Permeability of Magnetic Materials at Microwave Frequencies, *IEEE Transactions on Instrumentation and Measurement*. **39(2)**, 387-394.

[68] Simovski, C. R. (2009). Material Parameters of Metamaterials (A Review), *Optics and Spectroscopy*. **107(5)**, 726.

[69] Kim, S., Kuester, E. F., Holloway, C. L., Scher, A. D., Baker-Jarvis, J. (2011). Boundary Effects on the Determination of Metamaterial Parameters from Normal Incidence Reflection and Transmission Measurements, *IEEE Transactions on Antennas and Propagation*. **59(6)**, 2226-2240.

[70] Chen, X., Grzegorczyk, T. M., Wu, B. I., Pacheco Jr, J., Kong, J. A. (2004). Robust Method to Retrieve the Constitutive Effective Parameters of Metamaterials, *Physical Review E*. **70(1)**, 016608.

[71] Alù, A., Engheta, N., Erentok, A., Ziolkowski, R. W. (2007). Single-Negative, Double-Negative, and Low-Index Metamaterials and their Electromagnetic Applications, *IEEE Antennas and Propagation Magazine*. **49(1)**, 23-36.

[72] Hasar, U. C., Buldu, G., Bute, M., Muratoglu, A. (2017). Calibration-Free Extraction of Constitutive Parameters of Magnetically Coupled Anisotropic Metamaterials Using Waveguide Measurements, *Review of Scientific Instruments*. **88(10)**, 104702.